

A TIME EFFICIENT ADAPTIVE GRIDDING APPROACH AND IMPROVED CALIBRATIONS IN FIVE-HOLE PROBE MEASUREMENTS

Jason Town

Graduate Research Assistant

Email: jet234@psu.edu

Cengiz Camci

Professor of Aerospace Engineering

ASME Fellow

Email: cxc11@psu.edu

Turbomachinery Aero-Heat Transfer Laboratory

Department of Aerospace Engineering

The Pennsylvania State University

University Park, Pennsylvania 16802

Abstract

Five-Hole Probe (FHP), being a dependable and accurate aerodynamic tool, is an excellent choice for measuring three dimensional flow fields in turbomachinery. To improve spatial resolution, a subminiature FHP with a cross-sectional diameter of 1.68mm is employed. The high length to diameter ratio of the tubing inherent to the probe design usually causes increased measurement times. Additionally, manual pitch and yaw calibration increases uncertainty. A new FHP pitch and yaw calibrator is designed and built to reduce the uncertainty of the measurements by precise, computer controlled movements and reduced calibration time. The calibrated FHP is then placed downstream of the Nozzle Guide Vane (NGV) assembly of a low-speed, large-scale, single-stage, axial flow turbine. The cold flow HP turbine stage contains 29 nozzle guide vanes and 36 blades that are fully instrumented. A fast and computer controllable traversing system is implemented using an adaptive grid method for the refinement of measurements in regions such as the vane wake, the secondary flows, and the endwall boundary layers. The current probe movement approach increases the possible number of measurement points in a two hour period from 336 to 868, an increase of 160%. Flow structures behind the NGV measurement plane are identified with high spatial resolution and reduced uncertainty. The automated pitch and yaw calibration using a computer controlled arm and the adaptive measurement grid approach introduced in this study is shown to be a highly effective way of accurately measuring complex flow fields found in an axial flow turbine research rig.

Introduction

Five-Hole Probes are used to determine the three components of the mean velocity vector, local total pressure, and local static pressure [1]. They work by selectively comparing pressure data from five ports on the probe. According to Treaster and Yocom [2], by comparing the pressure differences between these ports, flow velocity magnitude, pitch angle, yaw angle, total pressure, and static pressure can be simultaneously determined. However, this method is found to work in a range of $\pm 30^\circ$ of pitch and yaw angle. A method is suggested by Ostowari and Wentz [3], to increase the range to $\pm 85^\circ$ by using a nulling method of the probe. However, nulling is not always possible, especially in the tight clearances and rotat-

ing machinery such as the flows internal to a turbine research rig. Norwack attempts to increase the range at which a FHP may be used by developing a long, spherical probe [4]. The useable range of the probe is increased to $\pm 65^\circ$, but the increased size make it hard to incorporate in many cases.

Correction methods by interpolation to find the necessary coefficients have been implemented through a variety of methods. A curve fitting approach is used by Treaster [2] and Weiz [5]. The curve fitting approach takes into account that the data taken by each port is in a different location. By using an orthogonal grid the data is curve fitted across the measurement region and interpolated to the center port of measurement. Reichert and Wendt suggest another method of data reduction for the FHP [6]. This method replaces the pitch and yaw angles with unit vectors and develops a Taylor series based approach to find flow parameters.

Dominy and Hodson studied the effects of Reynolds Number extensively. Their study showed how probe design could affect Reynolds Number related errors [7]. Treaster and Yocum [2] also covered this feature and suggested that calibration should be made at the expected Reynolds Number or a correction factor must be used. Methods for the detection of abnormalities in the probe are suggested by Morrison et al. [8]. These suggestions aid in the identification of probe damage and flow alignment issues.

Investigations into the effect of near-wall measurements with five-hole probes were carried out by Treaster and Yocum [2] and Lee and Yoon [9]. Both have concluded that measurements should be taken at least two probe diameters away from the wall. Closer causes blockage by the probe and acceleration of the flow, leading to greater uncertainty in the measurement. If it is necessary to operate closer than this distance, Lee and Yoon provide guidelines to make such measurements [9].

A FHP might also be used in place of laser Doppler anemometers for wake measurements, Brophy et al. [10]. The main application the FHP would be in location where it would be difficult to use a laser, such as the rotating frame of reference in a turbine or in geometrically difficult to reach flow zones. Sitaram, Lakshminarayana and Ravindranath have performed a detailed study on which type of probe to use within the rotating frame of a single stage compressor research rig at the Pennsylvania State University [11]. Town and Camci presented their early observations about using a sub-miniature five-hole probe in an axial flow turbine rig in [12].

There are many recent studies in the development of FHP based aerodynamic measurement systems. Pissasale and Ahmed [13] presented a theoretical calibration approach for a FHP for highly three dimensional flows. They also worked on a novel method for extending the calibration range of FHPs for highly three dimensional flows [14]. Development of a functional relationship between port pressures and flow properties for the calibration and application of a multi-hole probe to highly three-dimensional flow was a topic of investigation in their 2004 paper [15]. Multi-hole probes can also be used in the determination of skin friction coefficient in turbulent flows, Lien and Ahmed [16].

The present paper presents significant improvements in FHP based aerodynamic measurements in four significant areas. The specific approach reduces the elapsed calibration time of a typical five-hole probe from 3 hours down to 65 minutes for a (9x9) carpet map of pitch and yaw coefficients because of the unique properties of the new computer controlled calibration mechanism. A second major improvement is in the spatial resolution of measurements in selected high gradient areas such as the boundary layers, wakes, tip vortices, and secondary flow dominated flow zones. The third important property of the present approach is in the improved accuracy of the measurements because of an improved calibration sys-

tem, the use of more accurate positioning of the probe, the use of highly improved present day transducers, and a careful selection of tubing. Finally the current approach reduces turbine facility run-time significantly. The new system increases the number of data points that can be collected in a two hour period from 366 points to 868 points, an increase of 160%.

Symbols

<i>AFTRF</i>	Axial Flow Turbine Research Facility	
$C_{P,pitch}$	Pitch Coefficient	$(P_5 - P_4)/(P_1 - \bar{P})$ (1)
$C_{P,static}$	Static Pressure Coefficient	$(\bar{P} - P_{static})/(P_1 - \bar{P})$ (2)
$C_{P,total}$	Total Pressure Coefficient	$(P_1 - P_{total})/(P_1 - \bar{P})$ (3)
$C_{P,yaw}$	Yaw Coefficient	$(P_2 - P_3)/(P_1 - \bar{P})$ (4)
<i>DAQ</i>	Data Acquisition Device	
\bar{P}	Average value of outside pressure points (Pa)	$(P_2 + P_3 + P_4 + P_5)/(4)$ (5)
P_1	Pressure point 1, Figure 1	
P_2	Pressure point 2, Figure 1	
P_3	Pressure point 3, Figure 1	
P_4	Pressure point 4, Figure 1	
P_5	Pressure point 5, Figure 1	
P_s	Static pressure at defined location (Pa)	
P_T	Total pressure at defined location (Pa)	
P_{static}	Local FHP measured static pressure (Pa)	
P_{total}	Local FHP measured total pressure (Pa)	
V_1	Transducer voltage measured at point 1, Figure 1	
V_2	Transducer voltage measured at point 2, Figure 1	
V_3	Transducer voltage measured at point 3, Figure 1	
V_4	Transducer voltage measured at point 4, Figure 1	
V_5	Transducer voltage measured at point 5, Figure 1	
V	Absolute velocity magnitude (m/s)	
c	Calibration constant (Pa/V)	
<i>exit</i>	Measurement location downstream of rotor	
<i>inlet</i>	Measurement location upstream of NGV	
<i>local</i>	Measurement location in intraspace at specific point	
r	Radius to probe traverser track	
u	Velocity component in the probe relative x-direction (m/s)	
v	Velocity component in the probe relative y-direction (m/s)	
w	Velocity component in the probe relative z-direction (m/s)	
x	Distance of traverser from probe parallel to ground (zero) location	
z	Zero voltage measurement (V)	
α	Probe relative pitch angle ($^\circ$)	
β	Probe relative yaw angle ($^\circ$)	
θ	Desired measurement azimuthal angle	
ρ	Density (kg/m^3)	

Material and Methods

Objectives

First of the specific objectives is the reduction of elapsed calibration time of a typical FHP for use in the AFTRF from three hours down to about an hour for a (9x9) carpet map of pitch and yaw coefficient. A second major objective is in the improvements in the spatial resolution of measurements in selected high gradient areas such as boundary layers, wakes, tip vortices and secondary flow dominated zones. The third important objective of the present approach is in the improved accuracy of the measurements. The final objective is about significantly reducing the AFTRF turbine facility run-time for a selected FHP measurement effort.

Calibration Hardware

A flowchart for the acquisition of calibration data is shown in Figure 2. The commands, interface, and data logging at the computer level is written in LabVIEW. The 16-bit A/D converter system (DAQ) is made by Measurement Computing Corporation (MCC model USB-1608FS). It can obtain 200k samples per second, interfaces through USB, and has an accuracy of $\pm 0.68 \text{ mV}$ at an input range of $\pm 1 \text{ V}$. The 16-bit capabilities are essential to help reduce measurement uncertainty during the calibration and measurements.

The pressure is measured by a Validyne DP15 low pressure transducer with a 3500 Pa diaphragm. The transducer's accuracy is rated at 0.25 % , ($\pm 3.5 \text{ Pascal}$) of the full-scale measurement. Only one transducer is used to measure all five ports, its reference port is left open to atmosphere, and efforts are made to isolate the transducer thermally, electronically, and mechanically. Using one transducer for all five ports eliminates the bias errors coming from individual transducer zero values.

The transducer is connected to a Scanivalve Corp. 48-channel mechanical pressure selector. The specific electrical commands to step and reset the scanner are provided by the digital output D/A of the DAQ. The mechanical scanning approach with one transducer reduces measurement uncertainty by canceling out any thermal shift and calibration error the transducer might measure. It also reduces the total cost of the system, but comes at with increased measurement time for the calibrations and measurements.

Previously employed methods of pitch and yaw calibration were applied by hand. To increase the accuracy of movements, and decrease the total time taken for a complete calibration map, computer actuated rotary tables for pitch and yaw movements are used. Two different rotary tables are used, both are provided by Velmex Inc. The larger of the two, model B4800TS, is used to change the pitch angle. For each half step it moves 0.0125° . A second table, model B5990TS, is used to for yaw adjustments. For each half step it moves 0.010° .

The calibration rig shown in Figure 3 is designed to minimize movement of the probe tip in the direction normal to the outlet of the wind tunnel. The design intent is to keep the probe tip as near the intersection of the pitch and yaw axes as possible. This reduces the arm length of the probe and its displacement within the calibration jet.

A sub-miniature FHP shown in Figure 1 is designed and created on site using five hypodermic needles. It has a square cross-section with one hole in the center surrounded by four others located above, below, left and right of the center. All sides of the probe have been beveled to a 45° angle, leaving the center port in a normal plane to the flow. The specific hypodermic needles reduce the size of the probe to a maximum

diameter of 1.68 mm at the tip. The inherently small diameter of hypodermic tubing and the long length of tubing lead to a very large length to diameter ratio. Sub-miniature FHPs usually require relatively long settling and data acquisition times. However the small tip size increases the spatial resolution of the measurements and allows the probe to be inserted into the complex internal flow areas of most turbomachinery passages. An additional Pitot probe is also used to measure the calibration tunnel's free jet axial velocity, total pressure, and static pressure.

The calibration facility, shown in Figure 4, consists of an open loop wind tunnel with an axial blower, a diffused housing with multiple screens, a plenum chamber, a high area ratio circular nozzle, a circular to square transition nozzle, and a section of constant cross-sectional duct. The compressor is 45.7 cm in diameter and is driven by a variable speed motor rated up to 7.5 kW . The tests are performed in the free jet just outside of the constant cross-sectional duct. Free jet velocities are continuously adjustable via an AC inverter up to 28 m/s . Turbulent flow characteristics in the test section can be adjusted to turbulence intensity values between 0.5% to 1.2% by use of calibrated screens and biplane turbulence promoters. Details of the test section flow quality can be found in Wiedner [1], Kim, Wiedner and Camci [17],[18], and Rizzo and Camci [19].

Calibration Technique

A modified version of the calibration/reduction technique of a non-nulling FHP used by Treaster and Yocom [2] is used in this paper. The main difference between the two methods is in the way pitch and yaw angles are defined. Figure 1 defines the positions of the holes, the coordinate system for the probe, the positive angles of the probe, and the positive velocity components. In this configuration, being positioned on the probe facing the incoming flow, a positive pitch value would occur when the flow was coming from below the probe (nose up). Positive yaw value would occur when the flow is coming from the left (nose right). The only manual input into the calibration sequence is the initial hand positioning of the probe at zero pitch, zero yaw angles. The calibration grid uses an improved 81 point (9×9) configuration with more data points in the non-linear region near the maximum acceptance range of the probe ($\pm 30^\circ$). Calibration maps for coefficients of yaw, pitch, total pressure, and static pressure are calculated directly from the measurements of the FHP and Pitot probe as shown in Figures 8, 9 and 10. In most earlier studies the carpet maps were limited to a 49 (7×7) point configuration or less. One of the main concerns with calibrating a FHP is producing a high quality map with reduced absolute error. One concern is about instant changes in calibration flow quality that can be caused by laboratory disturbances or unwanted air currents. Another source of error can occur when the probe is first aligned with the flow. The probe is initially aligned by hand and is prone to human error. Only one transducer is used to sample pressure from all pressure measurement points. Five input channels to the rotary pressure scanner are required for the FHP ports and two input channels are needed for the Pitot probe documenting the total pressure and static pressure in the test section.

Using a single transducer for all seven pressure measurements during calibration measurably increased the elapsed time for a calibration. However, this approach significantly reduces calibration error. Equation 6 states that pressure is a function of the measured voltage V_n , the zero z , and a calibration factor c . Since the zero and the calibration factor are for only one transducer, they can be considered constant for all pressure measurements. The analysis will only take $C_{P,\text{total}}$ from Equation 3 into consideration, though it can be done with any of the other pressure coefficient equations. Substitution of Equation 6 into Equation 3 results in Equation 7. Since c is in every term, canceling it out leads to Equation 8. The result

of canceling out the z term in the numerator and simplifying the z term in the denominator is shown in Equation 9. Finally, the z term in the denominator cancels out and the result is shown in Equation 10. The result shows that when calculating $C_{P,total}$, or for that matter any of the C_P values, the zero and calibration factors cancel out. Thus, using one transducer eliminates the source of error that could be caused by a typical calibration of a transducer and incorrect zeroing procedure.

$$(6) \quad P_n = (V_n - z)c$$

$$(7) \quad C_{P,total} = \frac{(V_1 - z)c - (V_T - z)c}{(V_1 - z)c - \frac{(V_2 - z)c + (V_3 - z)c + (V_4 - z)c + (V_5 - z)c}{4}}$$

$$(8) \quad C_{P,total} = \frac{(V_1 - z) - (V_T - z)}{(V_1 - z) - \frac{(V_2 - z) + (V_3 - z) + (V_4 - z) + (V_5 - z)}{4}}$$

$$(9) \quad C_{P,total} = \frac{V_1 - V_T}{(V_1 - z) - \frac{V_2 + V_3 + V_4 + V_5 - 4z}{4}}$$

$$(10) \quad C_{P,total} = \frac{V_1 - V_T}{V_1 - \frac{V_2 + V_3 + V_4 + V_5}{4}}$$

Calculating Unknown Flow Variables

A FORTRAN code developed in-house is the traditional method of data reduction in the measurements of a FHP. The recent fully automated LabVIEW implementation of the same analytical calibration/reduction procedure is shown to produce identical results or better when compared to our past manual calibration/reduction system. Input to the code requires the current ambient temperature (T), absolute static pressure (P_s), and the five pressures as measurements of the FHP. The program then determines the pitch angle α through a series of linear interpolations. The interpolation scheme calls $C_{P,pitch}$ to be calculated for each possible pitch angle in the 81 point carpet map where there are nine possible pitch angles at a constant $C_{P,yaw}$. A second interpolation calculates the value of pitch angle by using the measured value of $C_{P,pitch}$. Yaw angle β is calculated in a similar interpolation scheme. This interpolation scheme calls $C_{P,yaw}$ to be calculated for each possible yaw angle at a constant $C_{P,pitch}$. The next interpolation calculates the exact value of yaw angle by using the measured value of $C_{P,yaw}$. A calibration chart used to visualize the data of the interpolations of pitch and yaw angle can be found in Figure 8.

Pitch and yaw angles are used for the interpolation of $C_{P,total}$ and $C_{P,static}$. The interpolation works similarly to pitch and yaw interpolation. First, α is held constant and an array of $C_{P,total}$, or $C_{P,static}$ is found with an array of β . The previously found value of β is then used to calculate $C_{P,total}$ and $C_{P,static}$ respectively. The charts used for the calculation of $C_{P,total}$ and $C_{P,static}$ can be found in Figures 9 and 10.

$$P_{total} = P_1 - C_{P,total}(P_1 - \bar{P}) \quad (11)$$

$$P_{static} = \bar{P} - C_{P,static}(P_1 - \bar{P}) \quad (12)$$

$$V = \left[\frac{2(P_T - P_S)}{\rho} \right]^{1/2} \quad (13)$$

$$u = V \cdot \cos \alpha \cdot \cos \beta \quad (14)$$

$$v = V \cdot \sin \beta \quad (15)$$

$$w = V \cdot \sin \alpha \cdot \cos \beta \quad (16)$$

Equations 3 a can be rewritten to solve for total and static pressure. The results are shown in Equations 11 and 12. Pitch and yaw angles are the first values found in the data reduction and are known. Definitions of velocity components with conventions are given in Figure 1 and derivations are in Equations 14, 15 and 16.

Axial Flow Turbine Research Facility

The Axial Flow Turbine Research Facility at Pennsylvania State University currently consists of a single stage state of the art HP turbine with 29 Nozzle Guide Vanes (NGV) and 36 rotor blades. Figure 5 shows a cross-sectional view of the AFTRF. Flow enters through the inlet bellmouth, and accelerates through the NGV. A detailed explanation of the design and characteristics of the AFTRF can be found in Lakshminarayana, Camci, Halliwell, and Zaccaria [20].

The recent probe traverser as shown in Figure 5 and Figure 6 is a modification of a previous design used in the AFTRF. In the previous design, circumferential movements were achieved by a belt system. The flexible belt system had noticeable play in it, and the new system replaces the belts with a precision built linear traverser shown in red. Replacing the belt system with a traverser greatly increases the accuracy and reduces the play of the system. There are two radial traversers that are connected to the trolley (light blue), and the probe holders are shown in yellow. It is designed with two radial traversers so that the system could take measurements in locations in between the NGV and rotor (intraspace), or downstream of the rotor. The new traversing system also includes improvements to the stepper motor drivers, which helps the traverser to move much faster than previously.

A cylindrical coordinate system is used within the AFTRF. Movements of the trolley could be translated to azimuthal position by calculation of arc length. Equation 17 is the result of the calculation to find the distance the traverser must move to change to a particular azimuthal angle θ . All distances are derived from a zero angle, the probe is parallel to the normal of the traverser. The radius r is the distance to the surface of the track that the trolley rides upon. The final variable, x , is the distance that the traverser must move from the zero position. To move from 1° to 2° , x is calculated for both cases and the values are subtracted to find the correct distance.

$$x = \frac{r \cdot \tan \theta}{\sqrt{\tan^2 \theta + 1}} \quad (17)$$

Data is acquired by a modular National Instruments CompactDAQ system. The module used to measure the analog signals of the Validyne DP-15 pressure transducers is a 32 channel, 16-Bit NI 9205 data acqui-

sition system. Rotor speed measurements are obtained from a high resolution MIL-spec optical encoder from BAE Systems (Model H25) encoder attached to the rotor. A Velmex VXM drives the stepper motors. All data logging, traverser movements, data analysis, and data recording are completed by a custom LabVIEW script.

Although a conventional Scanivalve mechanical pressure scanner was used in the calibration of the FHP measurements for the improved calibration accuracy, our current AFTRF FHP measurements are performed using state-of-the-art electronic pressure scanners. Thirty-two channel ZOC22b units from Scanivalve Corporation were employed in most of the turbine runs for faster operation and better thermal stability of the measurements.

Calculation of density in our FHP based calibrations and actual measurements require a measurement of local temperature. A K type thermocouple based probe is employed in our temperature measurements throughout the AFTRF. The thermocouple signal is referenced/amplified and converted into engineering units in a custom NI-9213 thermocouple processing unit. Our final temperature measurement accuracy for calibrations and AFTRF is estimated to be around $\pm 0.15^\circ\text{C}$.

Fluid flow through the AFTRF varies in velocity to the extent that a probe calibrated for the inlet could not be used in the intraspace or rotor exit relative frame locations, but could be used in the rotor exit absolute frame of reference. Table 1 covers the values of midspan velocity in meters per second. Present measurements are performed in the intraspace location, so the probe is calibrated at about 66 m/s .

Table 1: Predicted Midspan Flow Speeds and Locations

Location	Inlet	Intraspace	Absolute Exit	Relative Exit
Midspan Velocity (m/s)	16.15	66.30	20.05	66.88

Results

Five-Hole Probe Calibration

The carpet map as shown in Figure 7 was obtained four times in subsequent runs in an effort to establish the repeatability of the calibration process. The center of each cross represents the average value, while the four points surrounding each cross represents the data collected from each run. Nearly all points within the $\pm 20^\circ$ range have good grouping and are close to the average value. In the outlying regions of the calibration, those greater than $\pm 20^\circ$, the grouping is not as tight and initial alignment errors are exacerbated. The star shaped carpet map shown in Figure 7 is not perfectly symmetrical because a dimensionally perfect and symmetrical FHP is very difficult to manufacture because of the probe's small size and the inherent machining imperfections.

Calculations of $C_{P,pitch}$ and $C_{P,yaw}$ are found directly though Equations 4 and 1. The results are used to interpolate pitch and yaw angle values with the help of the data presented in Figure 8 that is a typical averaged carpet map produced by the current automated calibration approach. Figure 9 presents the variation in $C_{P,total}$ with respect to pitch and yaw angle. Interpolation is done to find $C_{P,total}$ using the pitch and yaw found in the previous section. Similarly, Figure 10 provides $C_{P,static}$ as a function of pitch and

yaw. $C_{P,static}$ can be recovered from the FHP measurements using the previously found pitch and yaw angles.

Previous design of calibration called for the probe to be moved by hand. One of the major advantages of the current computer automated system is stepper motor driven movements. No longer relying on human movement allows for a much greater degree of accuracy. The stepper motor controller can move the turn-tables in steps as fine as 0.0125° . Once the initial zero pitch and zero yaw position is defined at the start of each run, the computer driven mechanism can move to a new position with excellent spatial resolution and accuracy.

Calibrations of a FHP by manual pitch and yaw angle adjustments are long and arduous tasks. Previously, a 49-point map in a manual calibration effort took at least three hours to complete since a high quality adjustment of each pitch and yaw angle required great care. When the design was changed to the current automated system, a 49-point map took 65 minutes, and an 81-point map took 100 minutes. Further reduction in elapsed time is seen if multiple transducers are used, at the cost of previously mentioned accuracy improvements with the single transducer approach. An 81-point grid with multiple transducers takes approximately 22 minutes to complete. Ensemble averaging from four individually obtained carpet maps can also be very easily obtained in the current computer driven system in a time efficient manner. Ensemble averaging is an excellent way of removing some of the error originating from initial alignment of the probe. Paying attention to properly recording the transducer zero voltages just before a turbine run starts is an effective way of improving accuracy in the multiple transducer approach.

The method of attachment of a FHP to the pitch and yaw calibrator is extremely critical. The style and quality of the mechanical attachment influences the movement of the probe and the value of the calibration. Large swings and displacements can produce large errors in the calibration from spatial non-uniformity, turbulence decay, or shear layer mixing. The calibrator in Figure 3 shows a design where the probe's tip is located near the intersection of the pitch and yaw rotational axes. The improved design makes the calibration more accurate and reduces the uncertainties.

Due to the nature of the design of the probe, the initial alignment must be performed by hand. This is because of the small size and unforeseen defects that make nulling the probe unfeasible. However, a few techniques are developed in order to increase the initial alignment accuracy. First, a plumb bob is used to align the calibrator base so that it is parallel to the exit of the wind tunnel. This helps to insure that the probe will be held normal to the exit of the wind tunnel and parallel to the streamlines in the pitch direction. Yaw angle alignment is done with the help of a visible, horizontal laser beam. Placing a piece of paper over the exit of the tunnel allows for comparison of the shape of the shadow of the probe. The shadow is then brought to its minimum size by making small adjustments with the yaw stepper motor. These two alignments are done at the beginning of every run.

An uncertainty analysis is prepared for the total pressure, the static pressure, and velocity as defined by Equations 11, 12 and 13. An adaptation of a method set forth by Taylor [21] is used. Equation 18 is an example of the total pressure uncertainty estimates. The other variables follow the same processes but are not presented for brevity.

$$\delta P_T = \left[\left(\delta P_1 \frac{\delta P_T}{\delta P_1} \right)^2 + \left(\delta P_2 \frac{\delta P_T}{\delta P_2} \right)^2 + \left(\delta P_3 \frac{\delta P_T}{\delta P_3} \right)^2 + \left(\delta P_4 \frac{\delta P_T}{\delta P_4} \right)^2 + \left(\delta P_5 \frac{\delta P_T}{\delta P_5} \right)^2 + \left(\delta C_{P,total} \frac{\delta P_T}{\delta C_{P,total}} \right)^2 \right]^{1/2} \quad (18)$$

$$\delta P_1 = \delta P_2 = \delta P_3 = \delta P_4 = \delta P_5 = \pm 5 \text{ Pa} \quad (19)$$

$$\delta C_{P,total} = \pm 1/2 (C_{P,total \max} - C_{P,total \min}) \quad (20)$$

Accuracy of the transducer is approximately $\pm 3.5 \text{ Pa}$. Due to additional equipment and the high length to diameter ratio of connecting tubes, the accuracy decreased to $\pm 5 \text{ Pa}$. This is expressed in Equation 19. The uncertainty of the total pressure coefficient needs to be estimated using Equation 20.

Total pressure uncertainty is shown in Figure 11 where the most accurate region of the measurement is located slightly to the left of the zero pitch, zero yaw location. This is due to small defects that are asymmetries in the probe tip shape. The 30° pitch, -30° yaw location sees a much larger variation in total pressure. The dashed box represents a $\pm 20^\circ$ region that is to help identify the range for which the probe is the most accurate. When taking measurements, the incidence angle of the flow to the probe is kept within this region.

Static pressure uncertainty at 20 m/s is shown in Figure 12. The uncertainty results are not symmetric due to imperfections in the probe. The uncertainty near the center is larger. This is most likely because of the way the static pressure is calculated. When the probe is aligned with the flow, the pressure each tap measures increases in magnitude. This also increases the amount of uncertainty through greater variability. When the probe is taking measurements near the maximum range, some of the pressure measurements decrease and the overall uncertainty is reduced.

Velocity uncertainty shown in Figure 13 has a minimum to the left of center. It reaches a maximum uncertainty greater than $\pm 2.5 \text{ m/s}$ at pitch 30° and yaw -30° . Uncertainty in the recommended $\pm 20^\circ$ range is below $\pm 0.8 \text{ m/s}$.

Figure 14 represents the relative velocity uncertainty. The smallest error is located to the left of center in the map, while the largest error is located near the edges. At pitch 30° , yaw -30° the error is greater than 10%. Within the dashed box range of $\pm 20^\circ$ no error is found to be greater than 4%. The estimated error in the range of $\pm 10^\circ$ is about 2% of the calibration tunnel velocity.

The preceding figures determine that the most ideal operation of this probe would be within the $\pm 20^\circ$ range that is defined by the dashed box. A pitch and yaw range of $\pm 30^\circ$ is also possible. However, the elevated measurement uncertainty should be carefully evaluated in this range.

AFTRF Intraspace Five-Hole Probe Measurement Results

The new traverser greatly reduced the amount of time it takes to move from one point to another. The maximum allowable testing period for the AFTRF was about two hours. In older previous experiments performed in the AFTRF, a 336 point mesh was used with the same sampling time for each measurement point. This mesh would take approximately two hours to complete and could not handle adaptive gridding. Improvements in the traversing system increased the number of points that are measured in a two hour period to 868. The adaptive mesh and traverser improvements increased the number of points taken by nearly 160% over the previously used meshing techniques for the same two hour test.

The addition of the adaptive grid approach into the mesh generation allows fine measurements in locations of greater interest and large gradients. The iterative process that is done for the adaptive gridding is currently manual. The initial grid of 165 points is shown in Figure 15. This grid is refined in areas of wake, boundary layer, and endwall vortices until the grid becomes what is shown in Figure 16. The refined grid of Figure 16 allows for less time to be spent in regions of less variation and more time spent in large gradient areas.

$$C_{P,\text{total}} = \frac{P_{T,\text{local}} - P_{T,\text{inlet}}}{1/2 \rho V_{\text{inlet}}^2} \quad (21)$$

$$C_{P,\text{static}} = \frac{P_{S,\text{local}} - P_{T,\text{inlet}}}{1/2 \rho V_{\text{inlet}}^2} \quad (22)$$

Coefficient of total pressure as defined by Equation 21 for one vane pitch (12.41°) is shown in Figure 17. In this figure, the more negative values "going toward blue" indicate greater total pressure loss. The boundary layer near the hub is very small. The probe at the zero span location is currently behind a backward facing step which reduces size of the boundary layer. The passage vortex of the hub centered in the blue region is in the range of θ , from -1° to 1° , and span 0.05 to 0.10. The vane wake is the yellow region of total pressure loss that curve though the measurement span. Above 90% span, the uncertainty is increased as the probe is nearing the slot. This slot is used to access the intraspace measurement plane and the boundary layer can be seen along with the casing passage vortex.

Coefficient of static pressure measured by the FHP in the intraspace of the AFTRF as defined by Equation 22 is shown in Figure 18. One can see the effects the secondary flows in Figures 17 and 18. The highest static pressure can be found near the hub, the lowest static pressure is found near the casing. The casing has greater uncertainty because the measurements are taken near the instrumentation slot. Static pressure over the midspan varies from being values of -23 to values of -28 .

Velocity magnitude measured by the FHP is shown in Figure 19. The highest velocity is found near the hub and velocity is reduced near the casing. The blue region in Figure 17 identified as the hub passage vortex appears here as a yellow deficit zone in velocity in the same location. Inspection can make out the outline of the vane wake, but it is not as clear as the hub passage vortex. Velocities are the lowest near the casing. This is an area of increased uncertainty due to its proximity to the instrumentation slot. The casing passage vortex and boundary layer can be identified.

Since local velocity is known at each measurement location, mass averaging can be performed with the FHP results. This is achieved by taking the entire measurement area, partitioning it into slices of constant radius, and then finding the mass average of each slice of constant radius. Mass averaged total and static pressure are reported in Figure 20. The effect of the hub passage vortex is seen in the five to ten percent span region causing a higher static pressure and a lower total pressure. For much of the span the total pressure remains near zero, while static pressure is becoming greater as it moves toward the casing. Near the casing total and static pressure measurements converge due to loss from the casing boundary layer, passage vortex, and the increased uncertainty of the instrumentation slot.

Figure 21 shows the pitch angle measured by the FHP. In this case a positive pitch angle means the flow is moving radially toward the center of the test rig, or from the casing to the hub. Here, the effects of the backward facing step can be seen as an increased alpha near the hub. The entire passage shows the flow

is moving from the casing toward the hub as shown in Figure 20. Interference from the instrumentation slot results in flow moving radially toward the hub near 100% span.

Mass averaged yaw angle is shown in Figure 22. The effect of the hub passage vortex is seen near 5% span as a quick increase and decrease in yaw angle. Near 100% span, a yaw angle decrease is seen from the casing boundary layer and casing passage vortex. Increased uncertainty in this region is due to the instrumentation slot.

The mass averaged components of velocity are shown in Figure 23. Azimuthal velocity β is the largest component of velocity. The fluid out of the NGV is highly swirled. A reduction in this velocity from the hub passage vortex can be seen from five to ten percent. Velocity near the casing boundary layer, casing passage vortex and instrumentation slot locally reduces the azimuthal component of velocity. A nearly constant and very small magnitude radial velocity is shown over the entire span, signifying the flow is moving toward the hub from the casing. Axial velocity is the highest near the hub passage vortex, slowly changes over the whole span, and then quickly drops in the presence of the casing boundary layer and instrumentation slot. The velocity magnitude closely follows the azimuthal component. The effects of the hub passage vortex can be found from five to ten percent, and the casing effects are also shown as a reduction in velocity.

Conclusions

A subminiature five-hole probe is calibrated using a newly designed automated pitch and yaw calibration system and an overview of various recent FHP implementations are given. The automated system reduces the amount of time for an 81 (9x9) point carpet map calibration from three hours to 65 minutes.

Ensemble averaging of multiple runs measurably reduces the uncertainty of FHP calibrations in carpet maps. Uncertainty is further reduced by realigning the probe at a zero pitch, zero yaw position with the help of a laser level and plumb bob for each calibration run.

Using only one transducer during calibration reduces calibration uncertainty by eliminating the zero and calibration terms.

The fully automated pitch and yaw calibrator is designed to reduce uncertainty caused by streamwise displacement of the probe by keeping the tip of the probe close to the intersection of the pitch and yaw rotational axis. The pitch and yaw calibrator uses state of the art mechanical components, stepper motors, indexers and computer controls to provide incremental angular changes in reduced time duration when compared to the conventional manual calibrator.

An uncertainty analysis is completed on the FHP calibration data. Within a $\pm 20^\circ$ range total pressure uncertainty is found to be less than $\pm 12 \text{ Pa}$, static pressure uncertainty is less than $\pm 5 \text{ Pa}$, and velocity uncertainty is less than $\pm 1 \text{ m/s}$ (4%).

A calibrated probe is placed into a large scale axial turbine research rig. The research rig AFTRF has a recently modified probe traverser, state of the art stepper motor drivers, pressure transducers and programming approach. The new traverser replaces the old belt driven traverser with a mechanical system op-

erated by a few linear translation stages. The new traversing system allows for effective adaptive gridding with much higher spatial resolution and position accuracy when compared to the belt driven system. The new system has increased the number of data points that can be collected in a two hour turbine run period from 336 points to 868 points, an increase of approximately 160%. Current system parameters are monitored in real-time using a graphical user interface allowing for ease in tracking and monitoring the results of the test.

The current adaptive grid definition is proved to the computer by the user in a manual manner. However the present system also allows a fully automatic/adaptive grid definition starting from a coarse grid measurement. The present system has capabilities to detect large and small gradients of measured quantities in a relatively coarse grid. The computerized approach can define the new time optimized adaptive grid without human intervention. Experiments of this fully automated measurement grid generation system are underway.

The current approach provides a much needed mass averaged flow measurement system since it can provide all three components of the velocity vector over an area of interest with improved accuracy.

The calibrated probe currently maps the flow field behind the NGV using the new traversing system along one vane pitch and full span. Typical NGV passage exit flow structures such as vane wake, boundary layer, and passage vortex within the field are identified. The adaptive gridding method allows for measurements locations in these flow structures to be increased, while areas of smaller gradients are coarser. This leads to a reduction in the amount of time required to measure one entire vane passage.

The present paper presents significant improvements in FHP based aerodynamic measurements in four significant areas. The specific approach reduces the elapsed calibration time of a typical five-hole probe. A second major improvement is in the spatial resolution of measurements in selected high gradient areas. The third important property of the present approach is in the improved accuracy of the measurements. Finally the current approach reduces turbine facility run-time significantly.

Figures

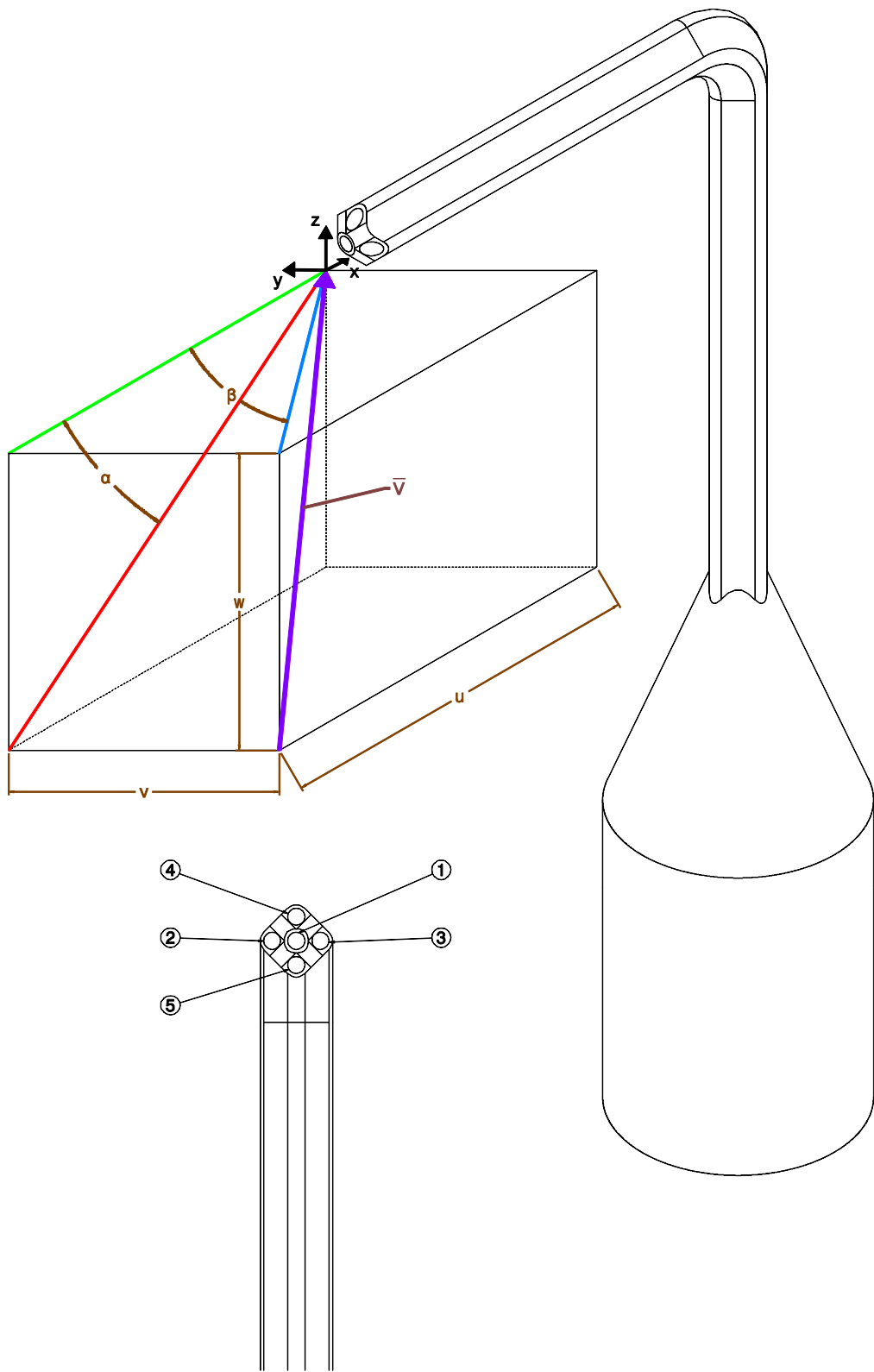


Figure 1: Isometric View of a Sub-Miniature Five-Hole Probe with Velocity Vector, Positive Angles, and Positive Velocity Components and Probe Port Number Assignments

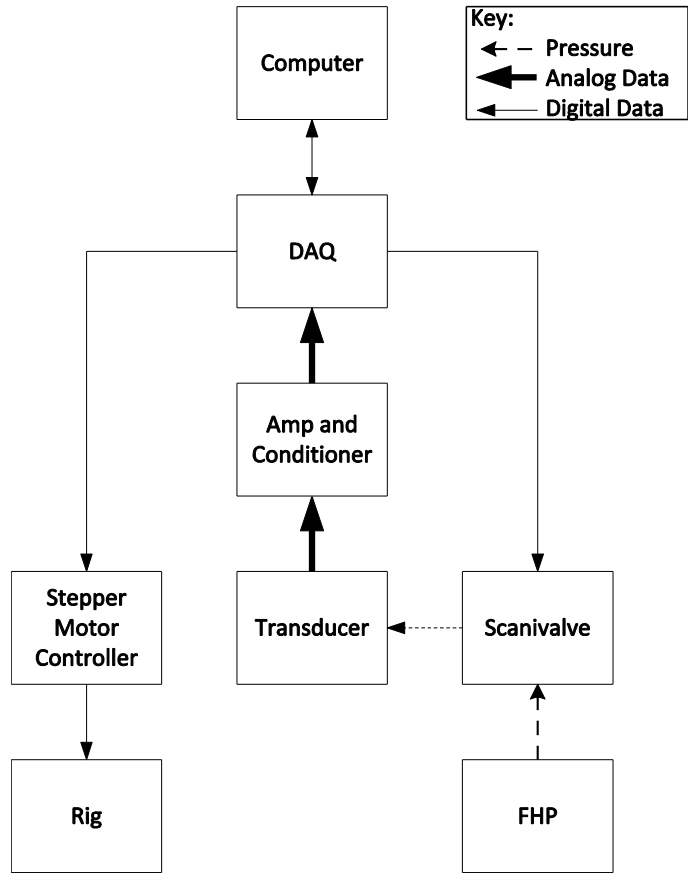


Figure 2: Calibration Block Diagram for Five-Hole Probe Measurements

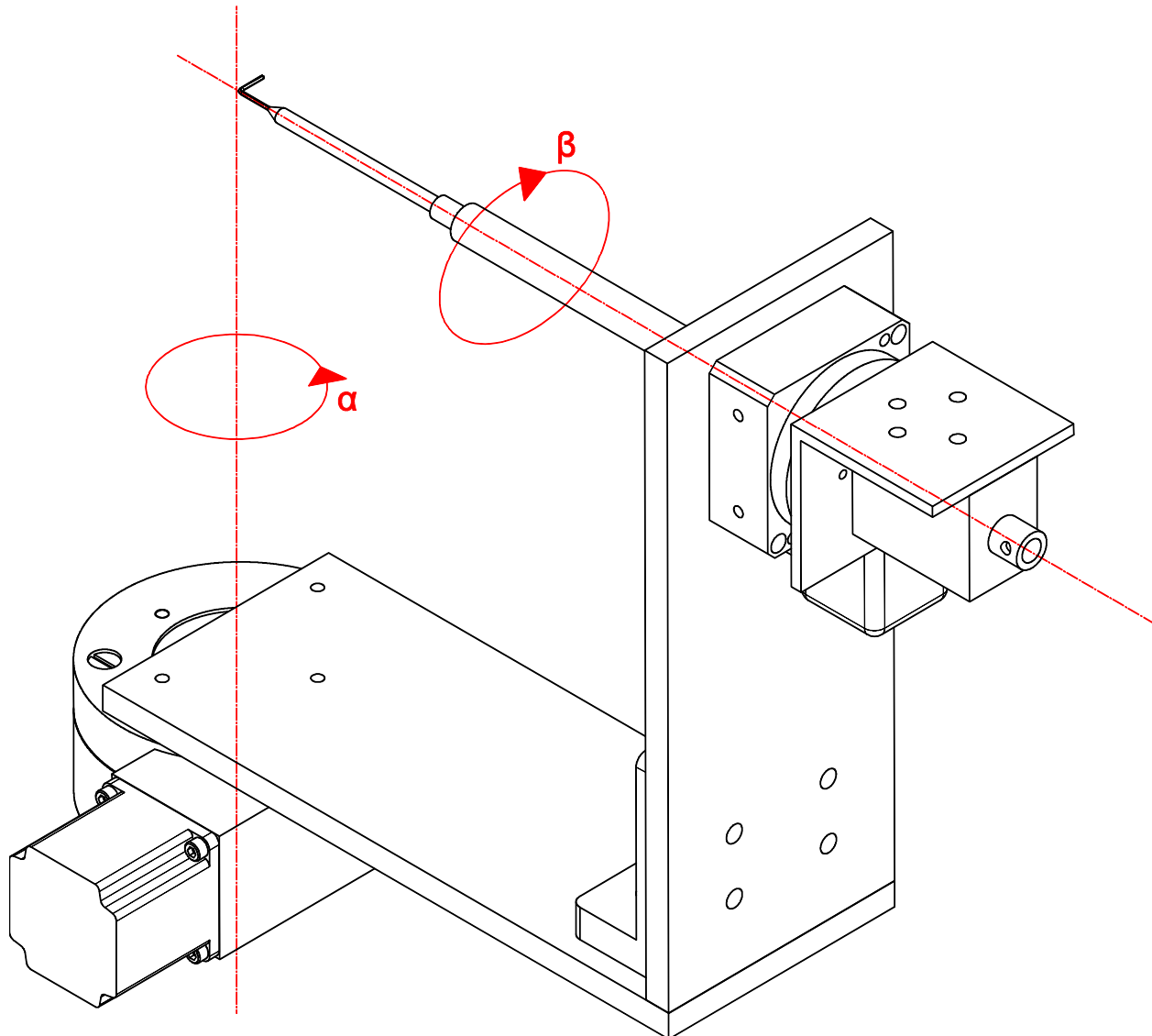


Figure 3: Calibrator Design with Pitch (α) and Yaw (β) Movements

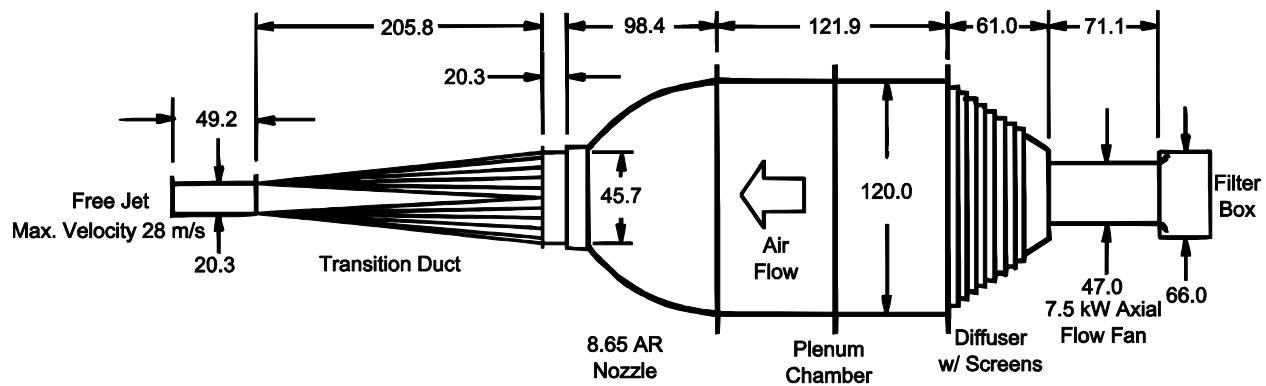


Figure 4: Calibration Wind Tunnel, Dimensions in Centimeters (Not to Scale)

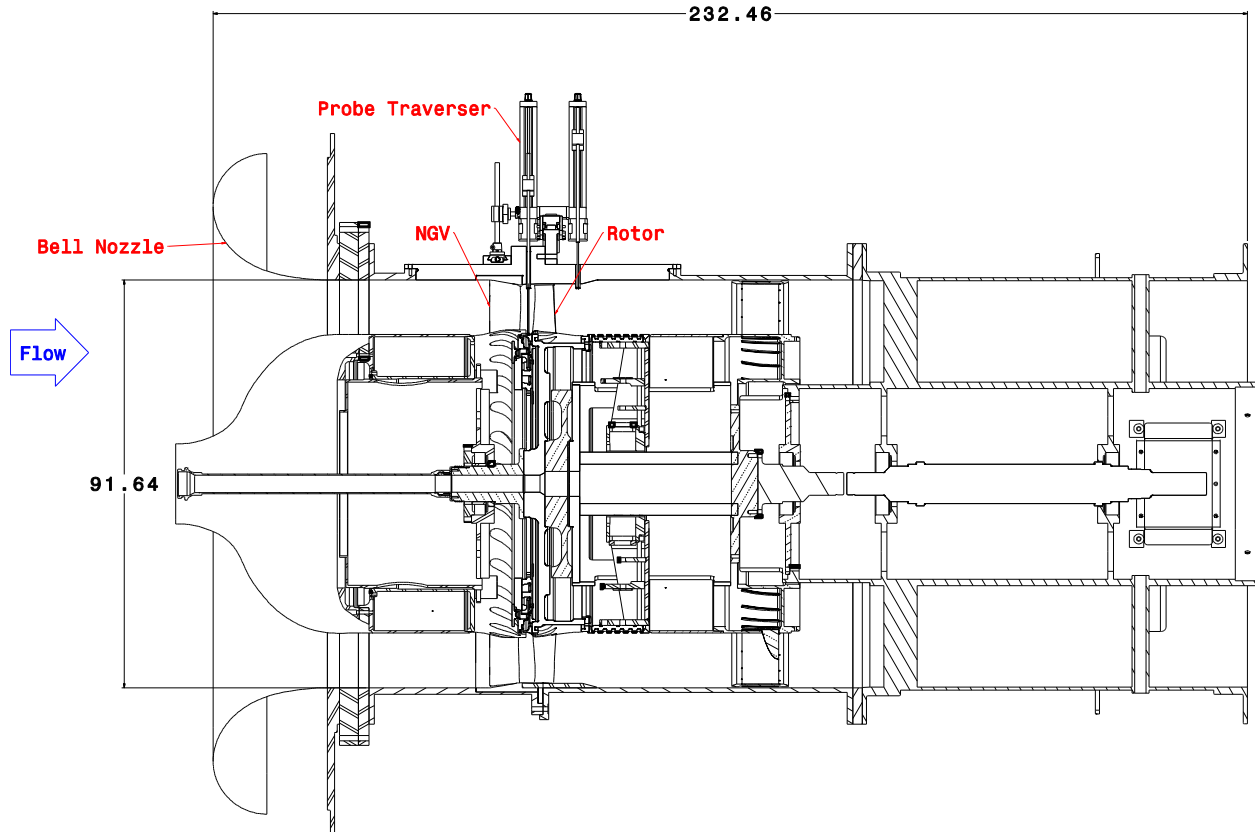


Figure 5: Axial Flow Turbine Research Facility (AFTRF) Cutaway (Dimensions in cm)

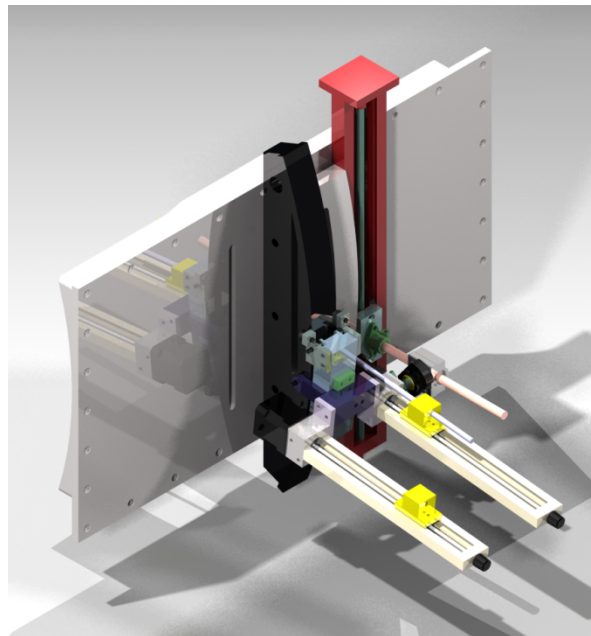


Figure 6: Probe Traverser Attached to the AFTRF Instrumentation Window, Isometric View

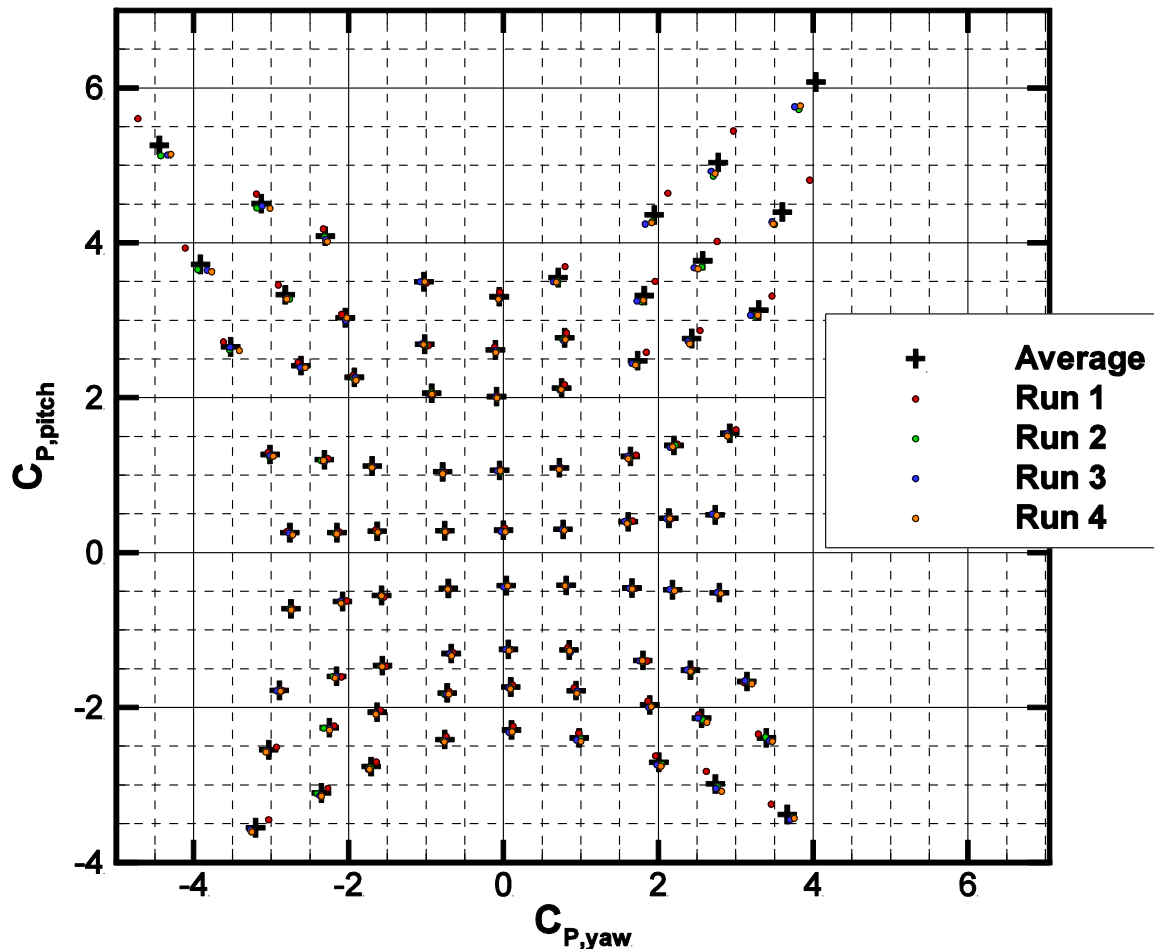


Figure 7: Average Values (Crosses) with Data Spread of Four Runs (Points)

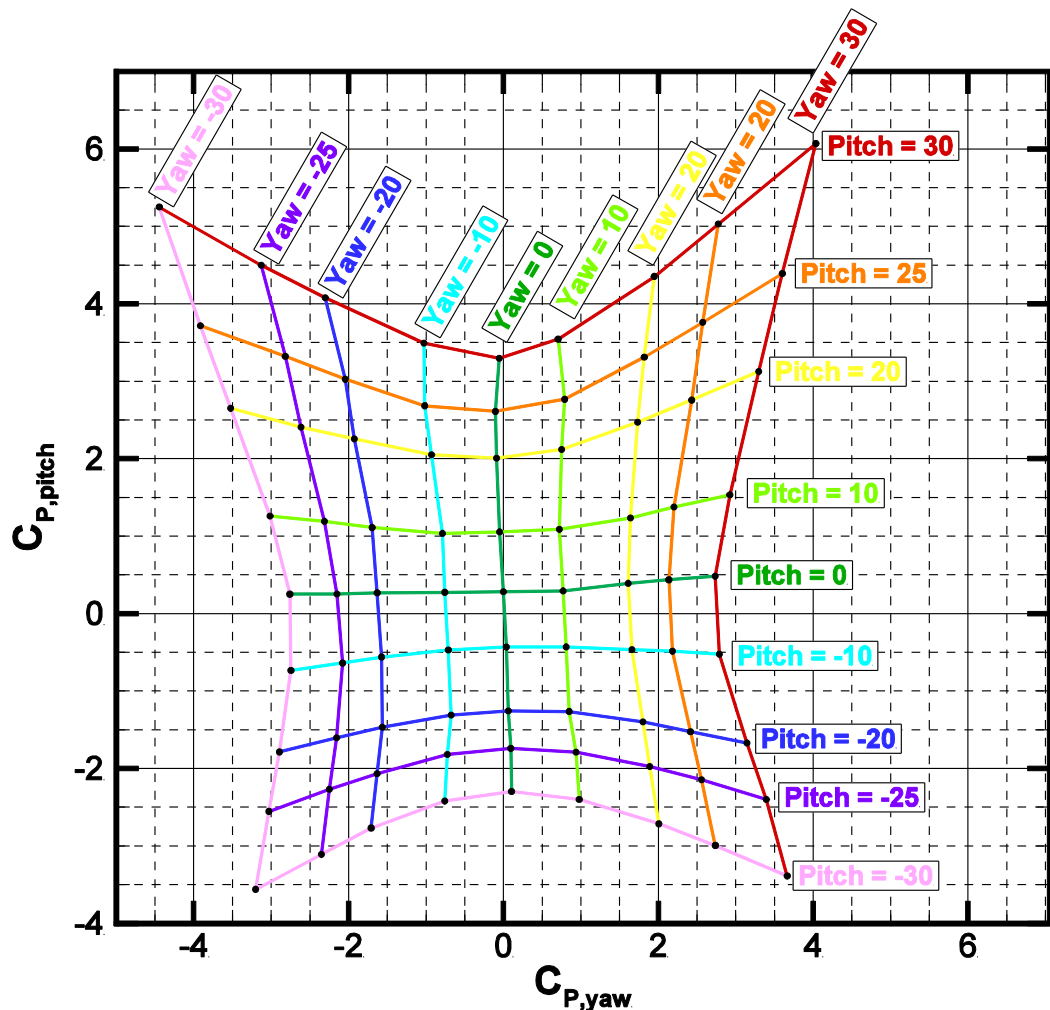


Figure 8: Coefficient of Yaw and Pitch with Lines of Constant Pitch or Yaw Angles, 81 (9x9) Points

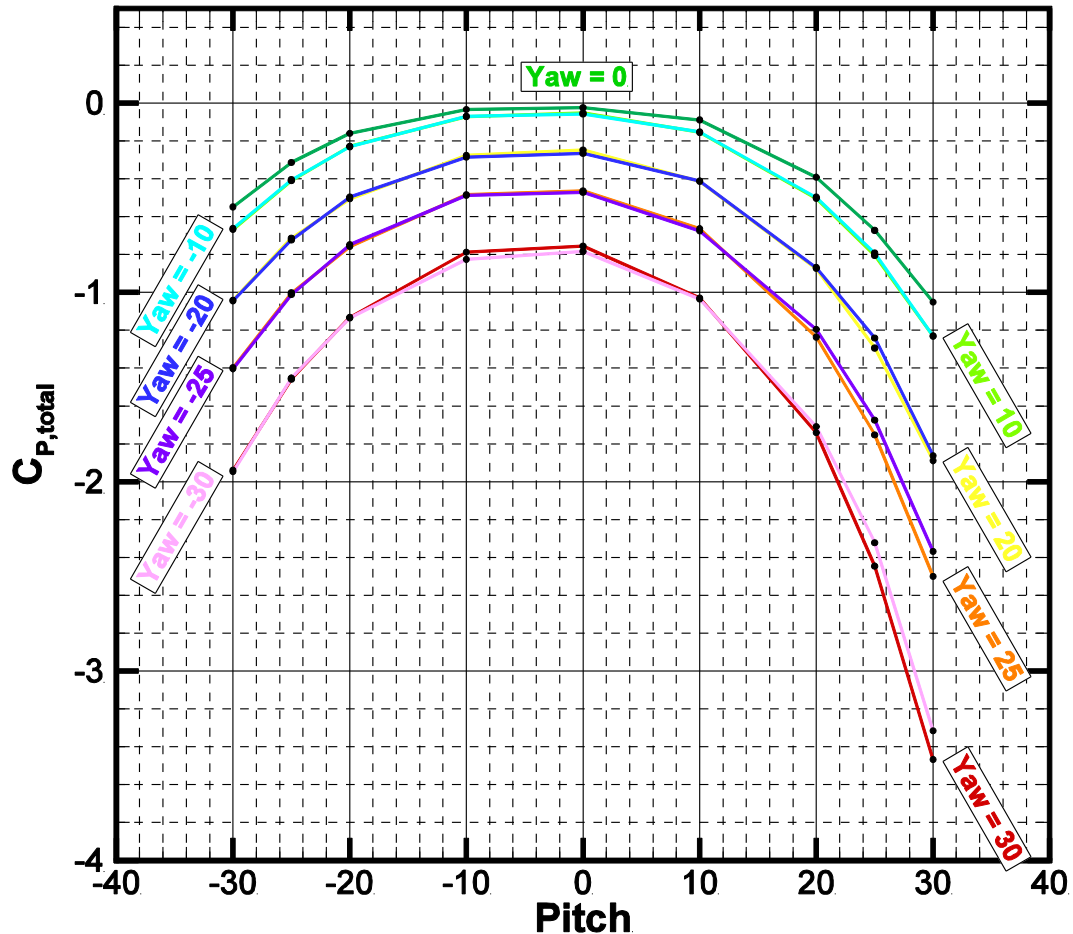


Figure 9: Pitch and Coefficient of Total Pressure with Lines of Constant Yaw, 81 (9x9) Points

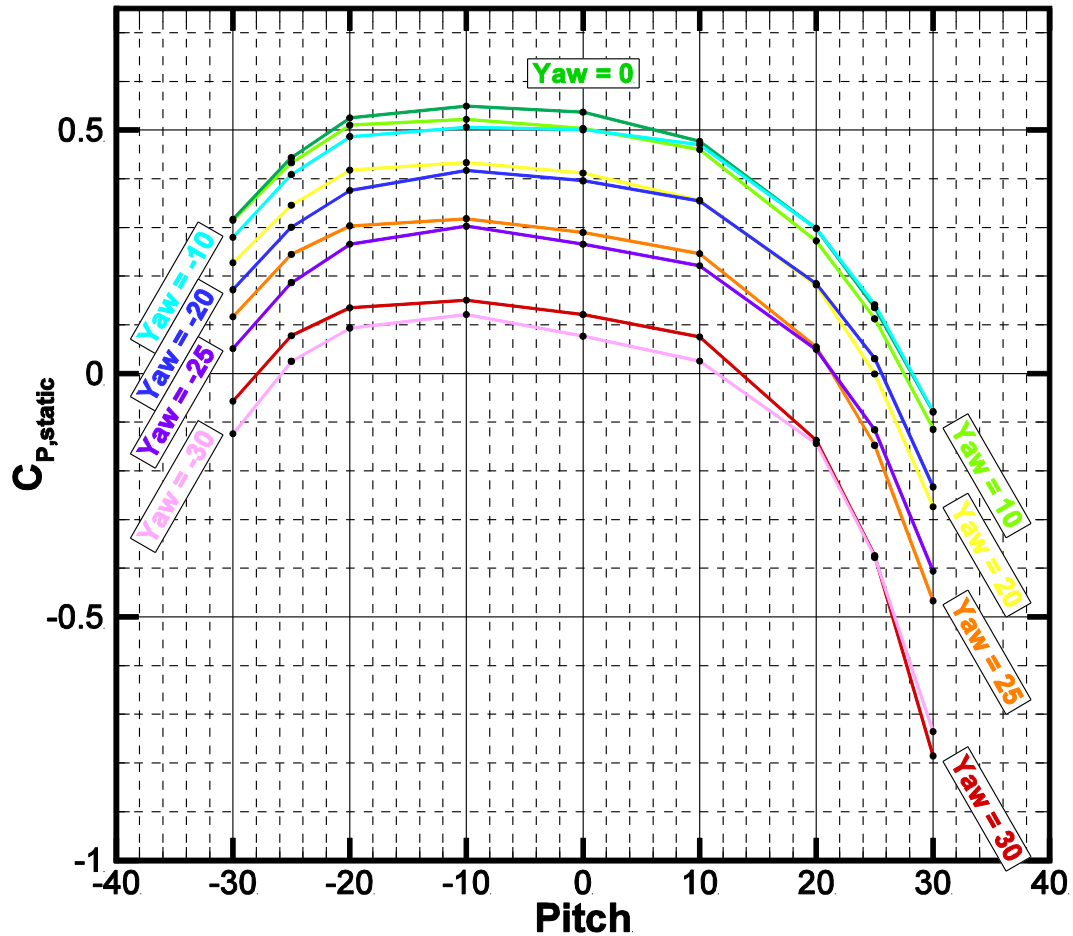


Figure 10: Pitch and Coefficient of Static Pressure with Lines of Constant Yaw, 81 (9x9) Points

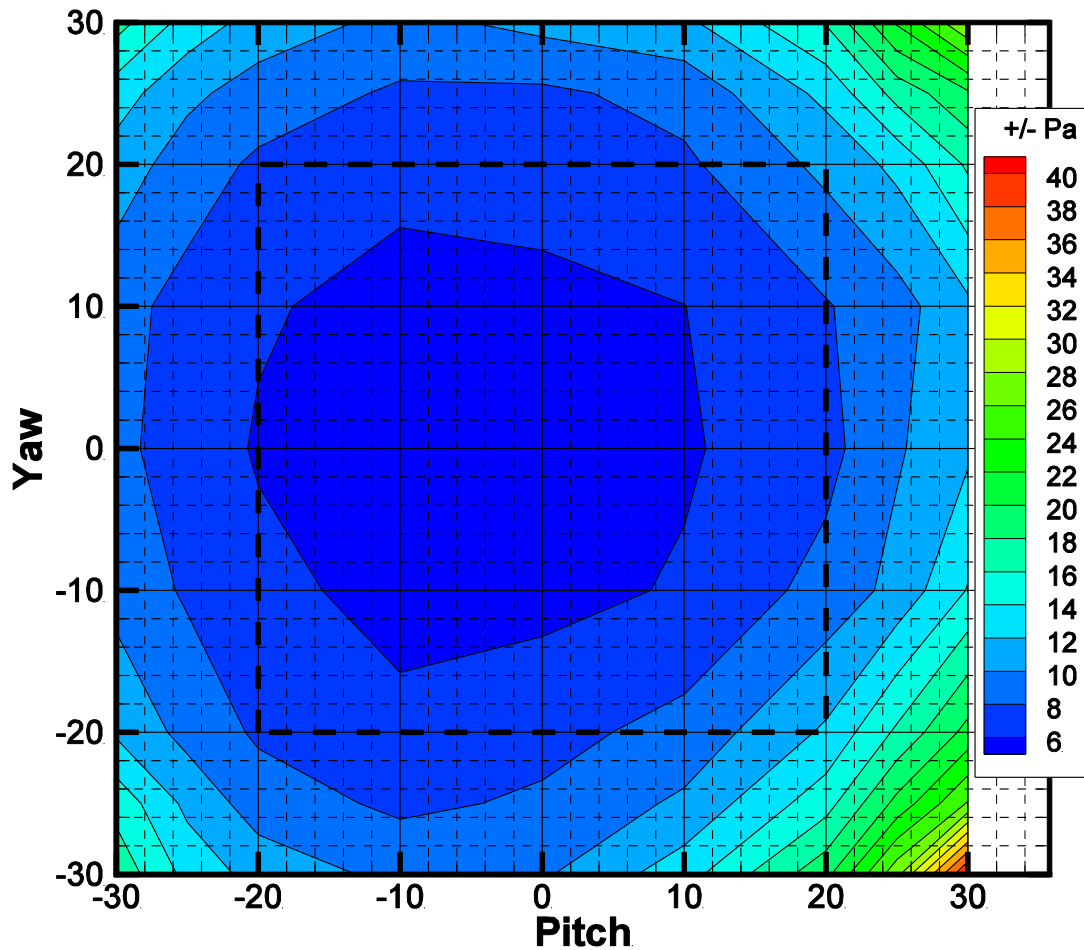


Figure 11: Total Pressure Uncertainty at 20 m/s , 81 (9x9) Points

(in terms of \pm Pa)

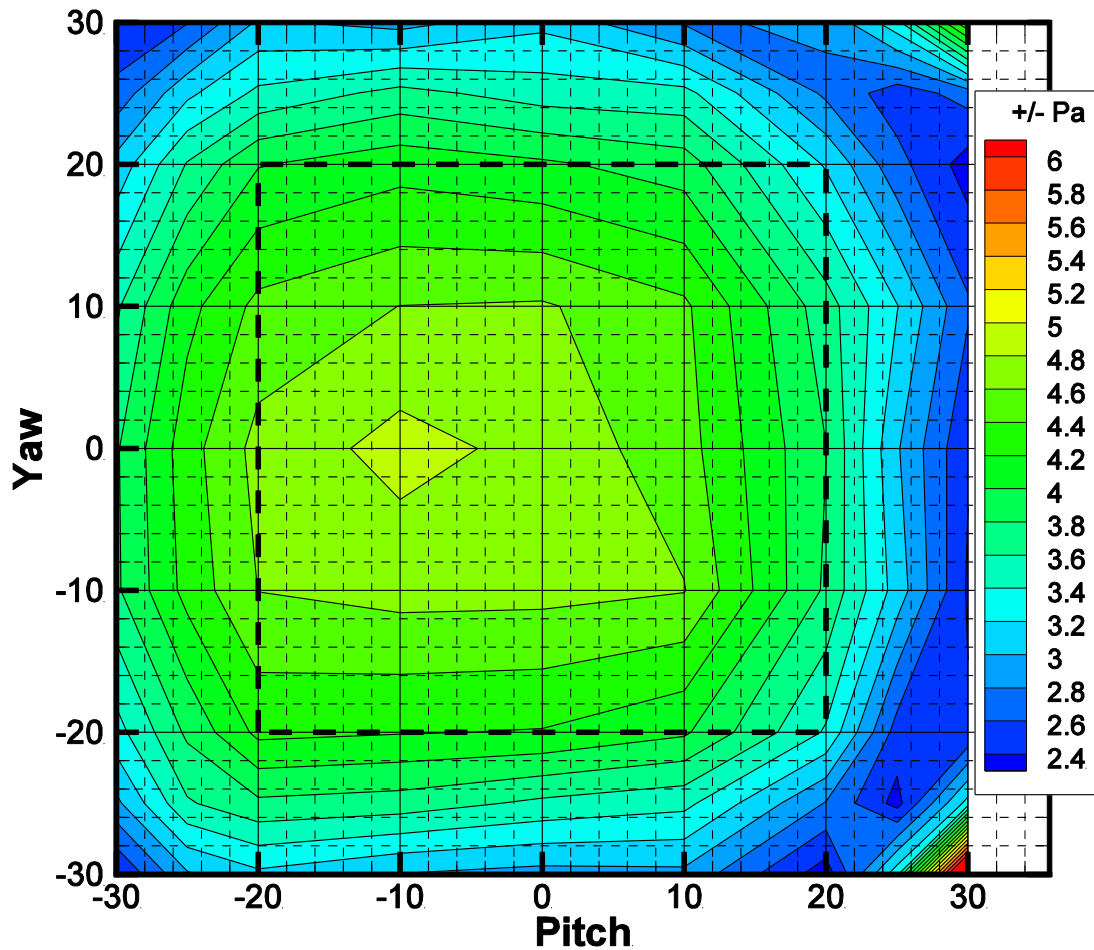


Figure 12: Static Pressure Uncertainty at 20 m/s , 81 (9x9) Points

(in terms of \pm Pa)

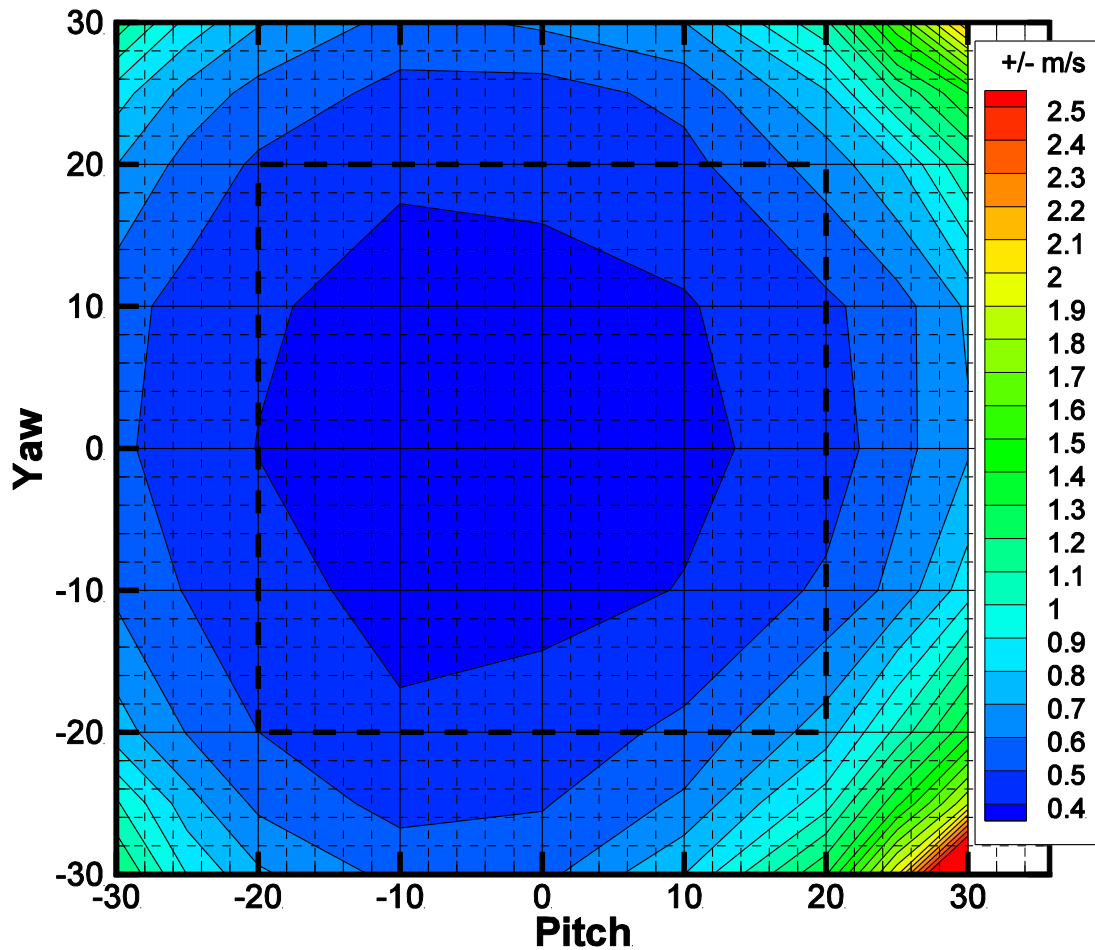


Figure 13: Velocity Uncertainty at 20 m/s , 81 (9x9) Points

(in terms of $\pm \text{m/s}$)

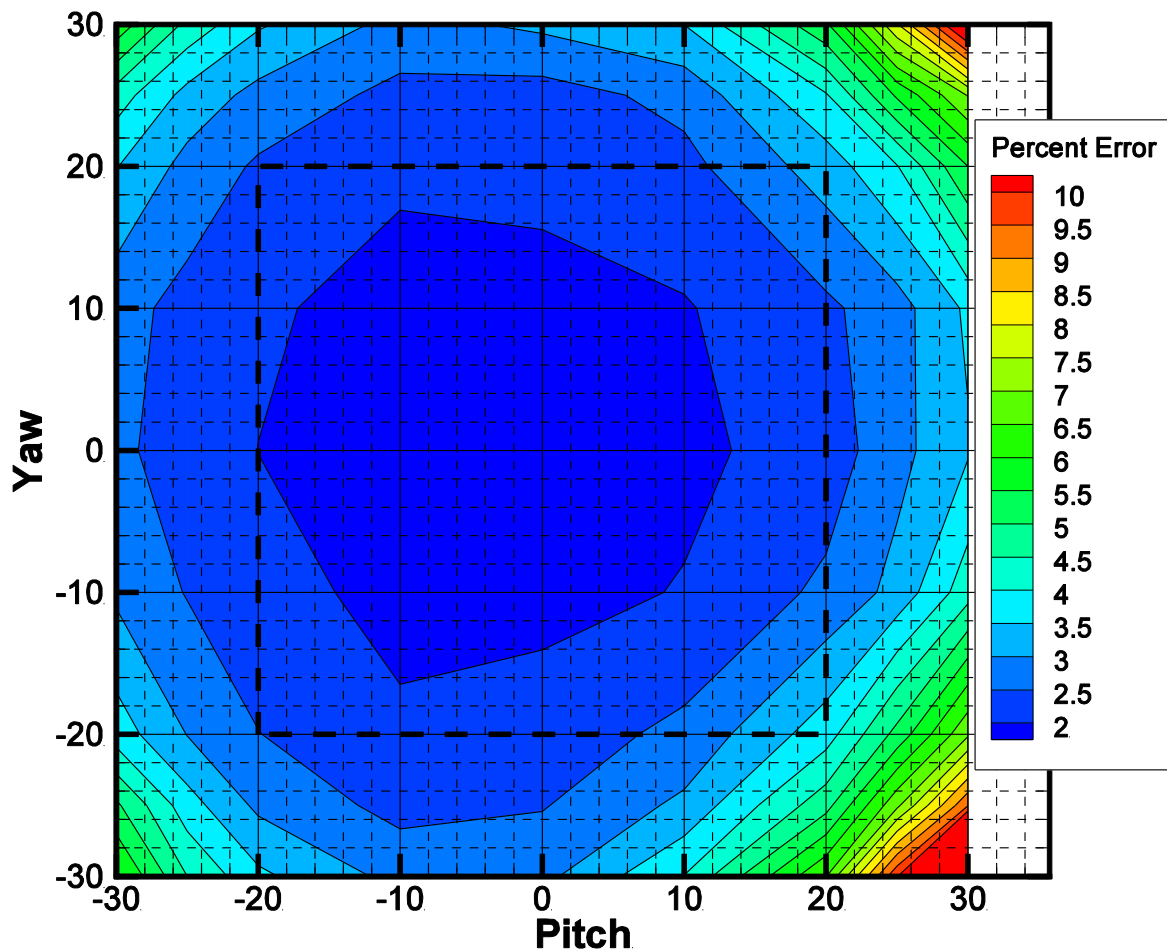


Figure 14: Velocity Percent Error at 20 m/s , 81 (9x9) Points

(in terms of percentage from baseline)

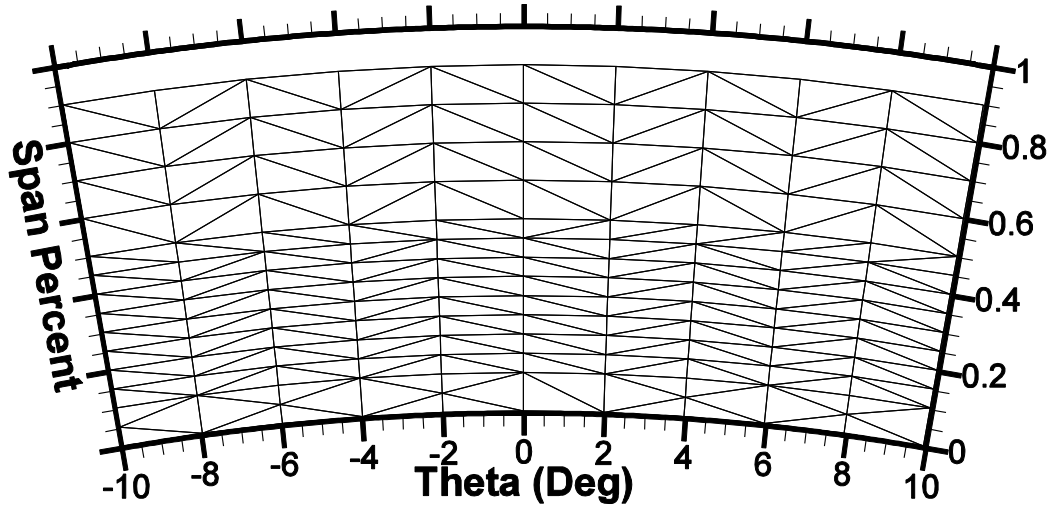


Figure 15: Initial Measurement Grid, 165 Points

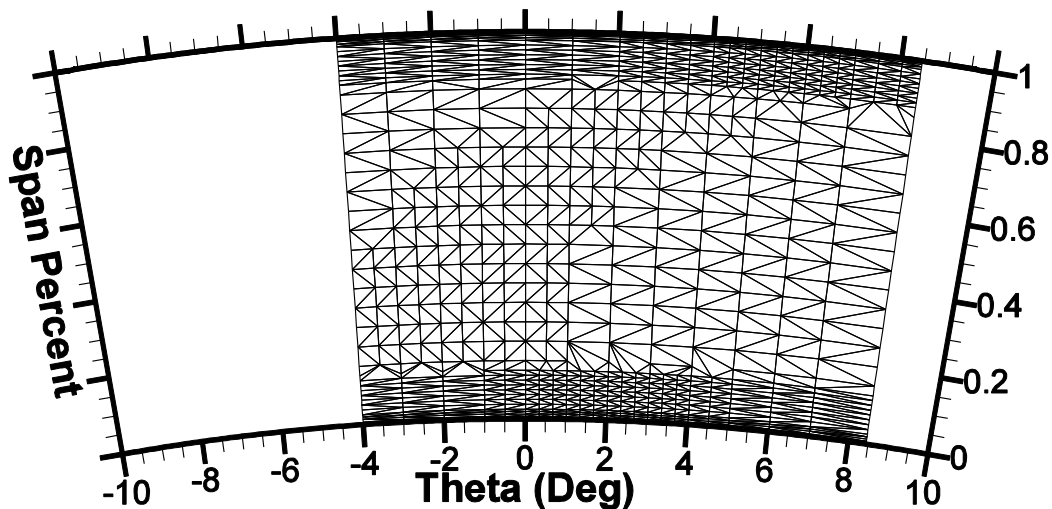


Figure 16: Refined Measurement Grid, 868 Points

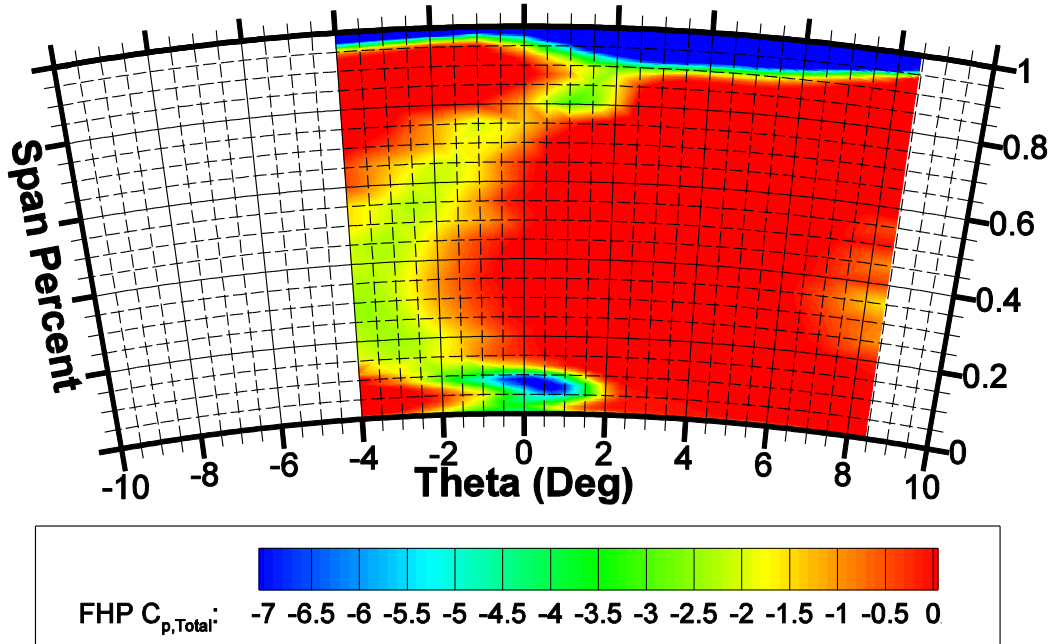


Figure 17: FHP Coefficient of Total Pressure, Intraspace

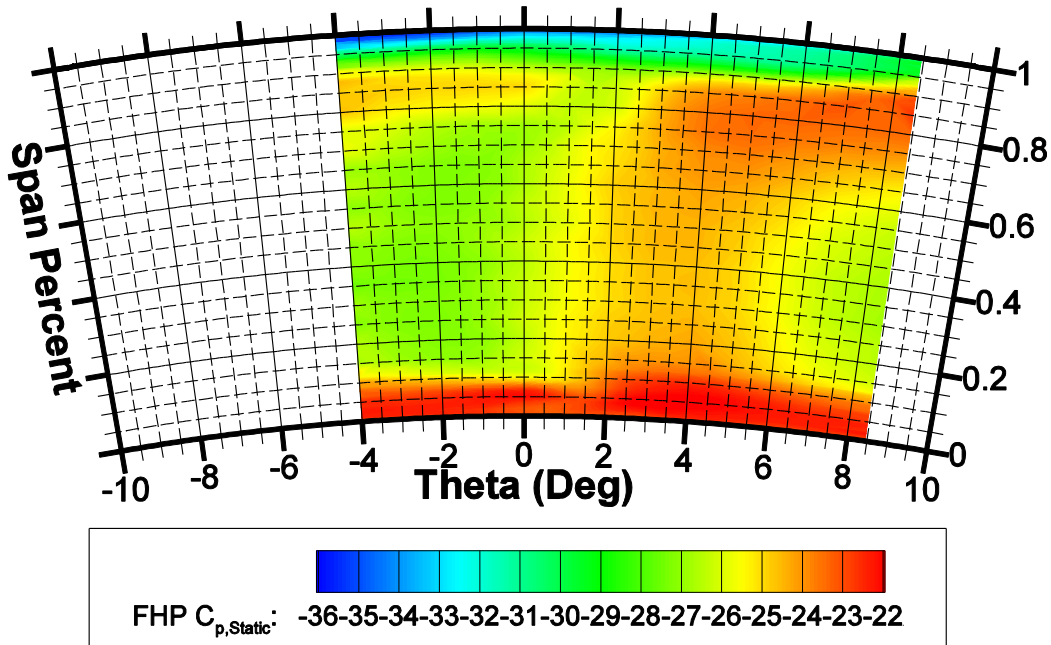


Figure 18: FHP Coefficient of Static Pressure, Intraspace

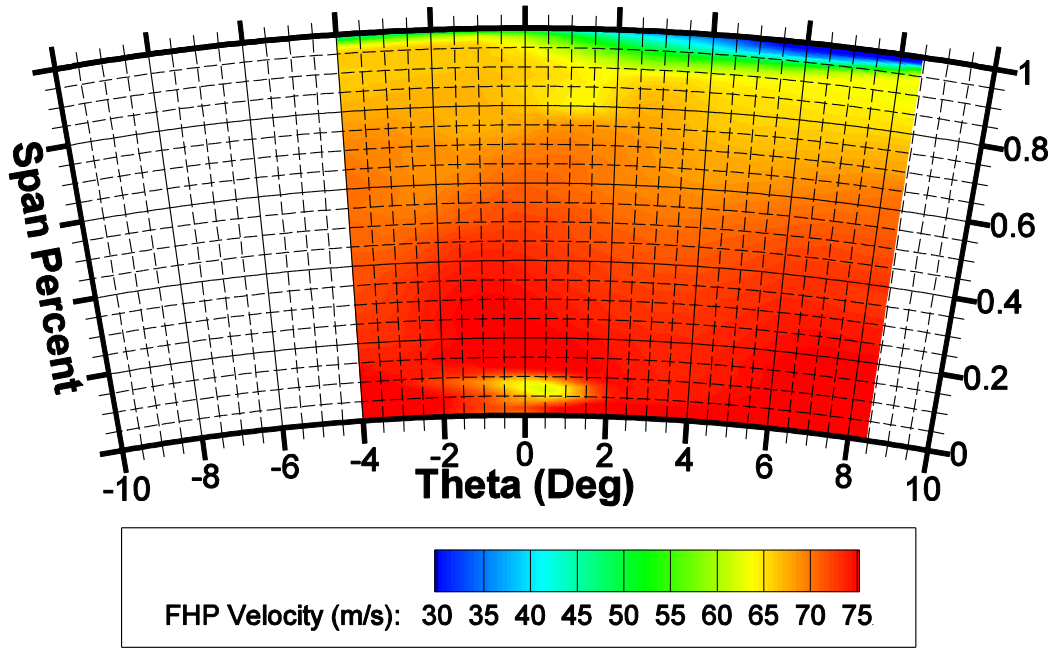


Figure 19: FHP Velocity Measurement, Intraspace

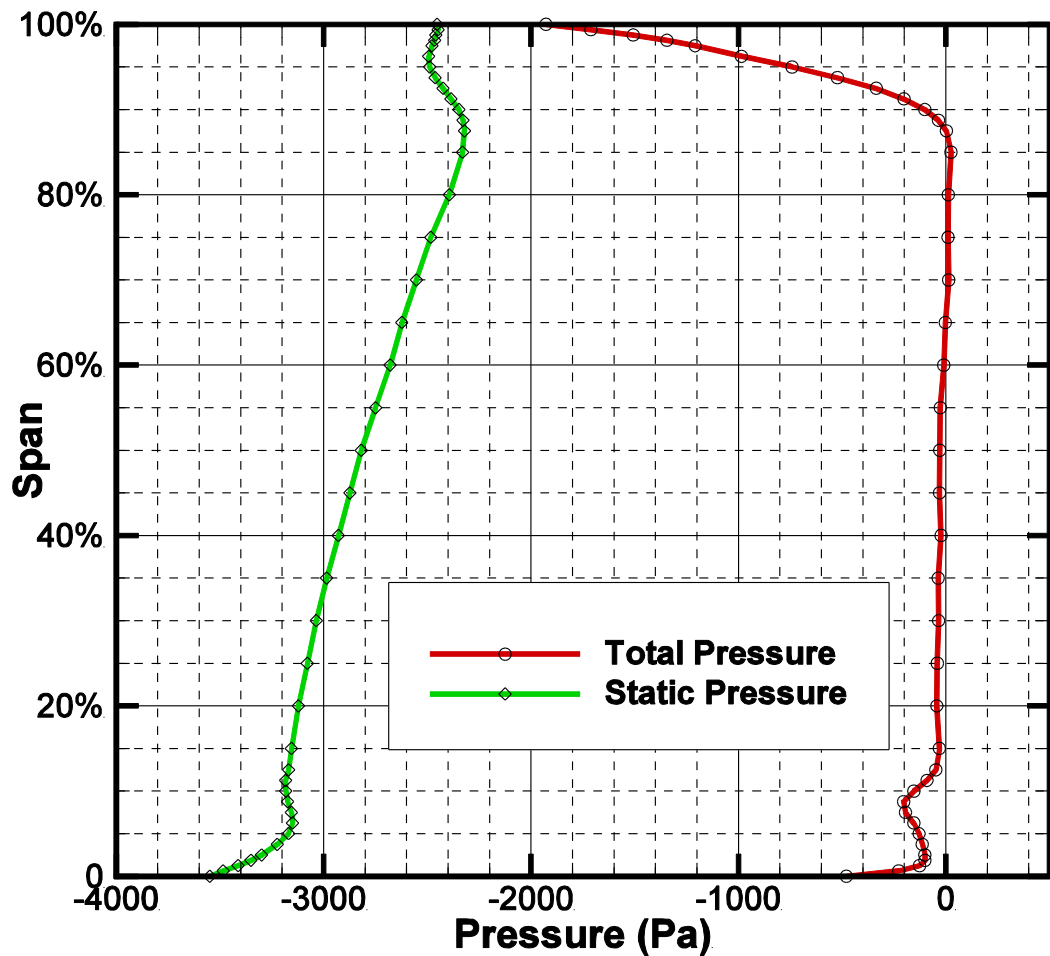


Figure 20: Mass Averaged FHP Measured Total and Static Pressure, Intraspace

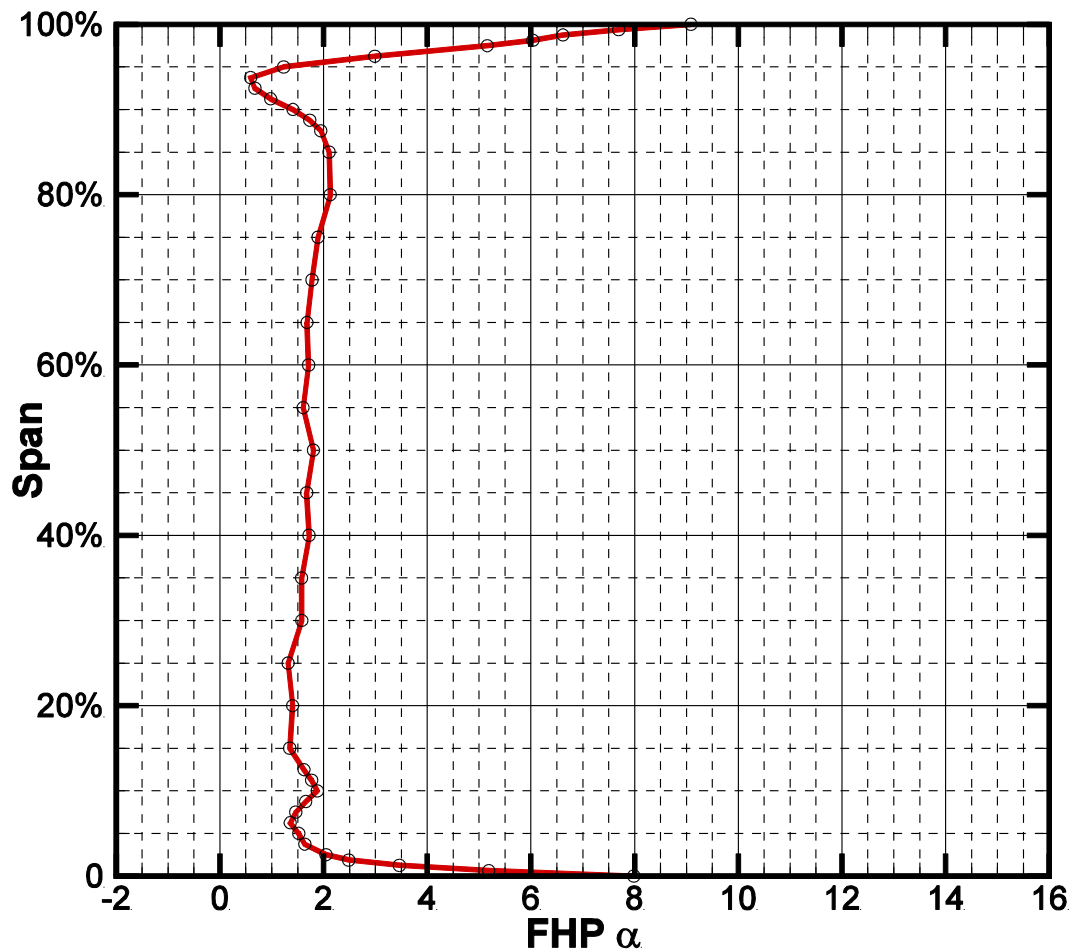


Figure 21: Mass Averaged FHP Measured Pitch (α) Angle, Intraspace

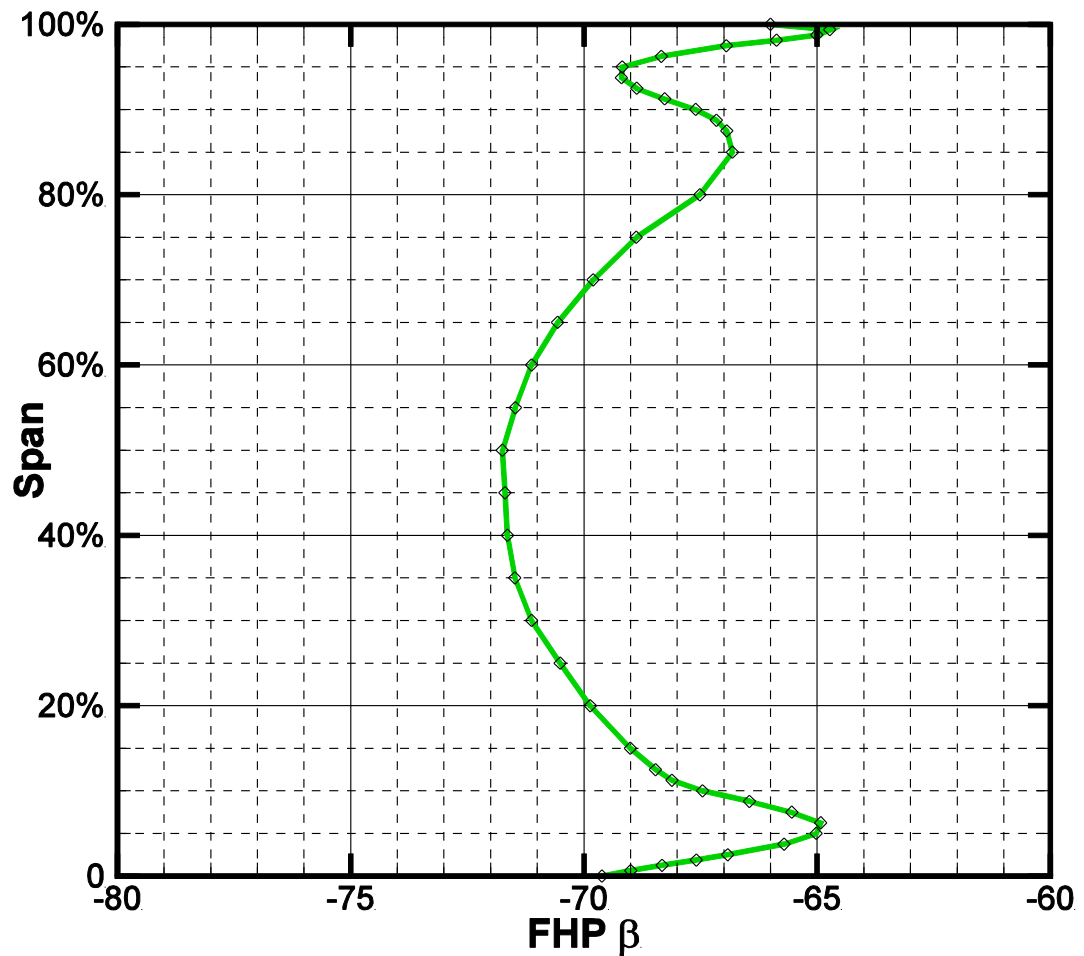


Figure 22: Mass Averaged FHP Measured Yaw (β) Angle, Intraspace

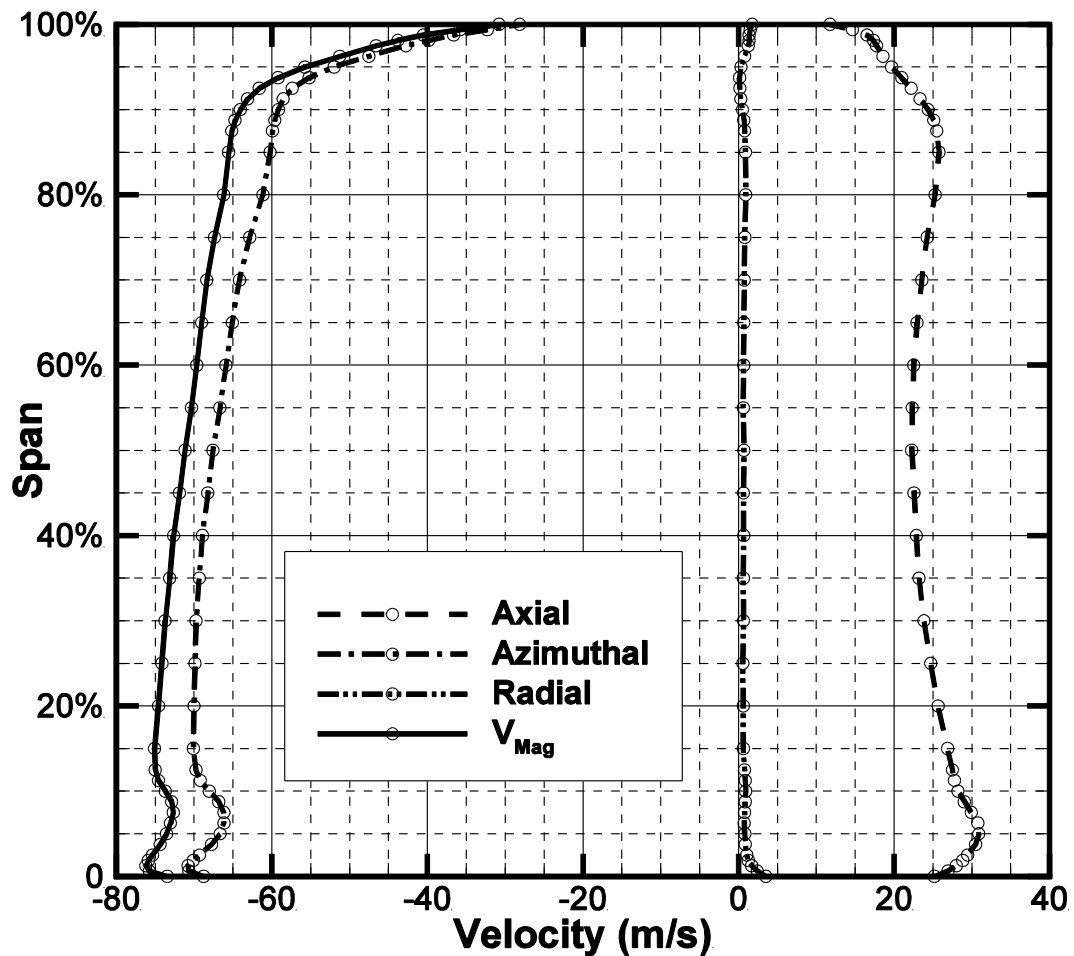


Figure 23: Mass Averaged FHP Measured Velocity Components, Intraspace

Works Cited

- [1] B. G. Wiedner, Passage Flow Structure and its Influence on Endwall Heat Transfer in a 90 Turning Duct, University Park: The Pennsylvania State University, 1994.
- [2] A. L. Treaster and A. M. Yocom, "The Calibration and Application of Five-Hole Probes," *ISA Transactions*, vol. 3, no. 18, pp. 23-34, 1979.
- [3] C. Ostowari and W. H. Wentz, "Modified Calibration Techniques of a Five-Hole Probe for High Flow Angles," *Experiments in Fluids*, vol. 3, no. I, pp. 166-168, 1983.
- [4] C. F. R. Nowack, "Improved Calibration Method for a Five-Hole Spherical Pitot Probe," *Journal of Physics E: Scientific Instruments*, vol. 1, pp. 21-26, 1970.
- [5] J. P. Weiz, "An Algorithm for Using the Five-Hole Probe in the Non-nulled Mode," The Applied Research Laboratory of the Pennsylvania State University, University Park, 1980.
- [6] B. A. Reichert and B. J. Wendt, "A New Algorithm for Five-Hole Probe Calibration and Data Reduction and Its Application to a Rake-Type Probe," ASME-FED Publications, 1993.
- [7] R. G. Dominy and H. P. Hodson, "An Investigation of Factors Influencing the Calibration of Five-Hole Probes for Three-Dimensional Flow Measurements," *Journal of Turbomachinery*, vol. 115, pp. 513-519, 1993.
- [8] G. L. Morrison, M. T. Schobeiri and K. R. Pappu, "Five-Hole Pressure Probe Analysis Technique," *Flow Measurement and Instrumentation*, vol. 9, pp. 153-158, 1998.
- [9] S. W. Lee and T. J. Yoon, "An Investigation of Wall-Proximity Effect Using a Typical Large-Scale Five-Hole Probe," *Korean Society of Mechanical Engineers International Journal*, vol. 3, no. 13, pp. 273-285, 1999.
- [10] M. C. Brophy, A. L. Treaster, D. R. Stinebring and J. P. Weiz, "Optimization of a Five-Hole Probe Wake Measuring System," Technical Memorandum 87-156, Applied Research Laboratory, The Pennsylvania State University, University Park, 1980.
- [11] N. Sitaram, B. Lakshminarayana and A. Ravindranath, "Conventional Probes for the Relative Flow Measurement in a Rotor Blade Passage," in *Proceedings of the Joint Fluids Engineering Gas Turbine Conference and Products Show, New Orleans, LA March 10-13, 1980*, New York, 1980.
- [12] J. Town and C. Camci, "Sub-Miniature Five-Hole Probe Calibration Using a Time Efficient Pitch and Yaw Mechanism and Accuracy Improvements," in *ASME GT-46391, ASME International Gas Turbine Conference*, Vancouver, 2011.
- [13] A. Pissasale and N. A. Ahmed, "Theoretical Calibration of a Five-Hole Probe for Highly Three Dimensional Flow," *International Journal of Measurement Science and Technology*, vol. 13, pp. 1100-1107, July 2002.

- [14] A. Pissasale and N. A. Ahmed, "A Novel Method of Extending the Calibration Range of Five-Hole Probe for Highly Three Dimensional Flows," *Journal of Flow Measurement and Instrumentation*, vol. 13, no. 1-2, pp. 23-30, March-April 2002.
- [15] A. Pissasale and N. A. Ahmed, "Development of a Functional Relationship between Port Pressures and Flow Properties for the Calibration and Application of Multihole Probes to Highly Three-dimensional Flows," *Experiments in Fluids*, vol. 36, no. 3, pp. 422-436, March 2004.
- [16] J. Lien and N. A. Ahmed, "An Examination of the Suitability of Multi-hole Pressure Probe Technique for Skin Friction Measurement in Turbulent Flow," *Journal of Flow Measurement and Instrumentation*, vol. 22, pp. 153-164, 2011.
- [17] K. Kim, B. G. Wiedner and C. Camci, "Turbulent Flow and Endwall Heat Transfer Analysis in a 90 Degree Turning Duct and Comparisons with Measured Data Part II: Influence of Secondary Flow, Vorticity, Turbulent Kinetic Energy, and Thermal Boundary Conditions on Endwall Heat Transfer," *International Journal of Rotating Machinery*, vol. 8, no. 2, pp. 125-140, 2002.
- [18] K. Kim, B. G. Wiedner and C. Camci, "Turbulent Flow and Endwall Heat Transfer Analysis in a 90 Degree Turning Duct and Comparisons with Measured Data Part I: Influence of Reynolds Number and Streamline Curvature on Viscous Flow Development," *International Journal of Rotating Machinery*, vol. 8, no. 2, pp. 109-123, 2002.
- [19] D. H. Rizzo and C. Camci, "Secondary Flow and Forced Convection Heat Transfer Near Endwall Boundary Layer Fences in a 90 Degree Turning Duct," *International Journal of Heat and Mass Transfer*, vol. 45, pp. 831-843, 2002.
- [20] B. Lakshminarayana, C. Camci, I. Halliwell and M. Zaccaria, "Design and Development of a Turbine Research Facility to Study Rotor-Stator Interaction Effects," *International Journal of Turbo and Jet Engines*, vol. 13, pp. 155-172, 1996.
- [21] J. R. Taylor, "An Introduction to Error Analysis the Study of Uncertainties and Physical Measurements," Sausalito, University Science Books, 1997, p. 75.
- [22] P. M. Ligrani, B. A. Singer and L. R. Baun, "Miniature Five-Hole Pressure Probe for the Measurement of Three Mean Velocity Components in Low-speed Flows," *Journal of Physics E: Scientific Instruments*, vol. 10, no. 22, pp. 868-876, 1989.
- [23] A. L. Treaster and H. E. Houtz, "Fabricating and Calibrating Five-Hole Probes," in *Proceedings of the Fourth Fluid Mechanics, Plasma Dynamics, and Laser Conference, Atlanta, GA, May 11-14, 1986*, New York, 1986.